Cationic lipid-conjugated dexamethasone as a selective antitumor agent

ARTICLE *in* EUROPEAN JOURNAL OF MEDICINAL CHEMISTRY · JUNE 2014

Impact Factor: 3.45 · DOI: 10.1016/j.ejmech.2014.06.051 · Source: PubMed

2 AUTHORS:

Samaresh Sau
Purdue University
6 PUBLICATIONS **7** CITATIONS
SEE PROFILE

Rajkumar Banerjee
Indian Institute of Chemical Technology
42 PUBLICATIONS **621** CITATIONS
SEE PROFILE

European Journal of Medicinal Chemistry 83 (2014) 433–447

Contents lists available at ScienceDirect

European Journal of Medicinal Chemistry

journal homepage: http://www.elsevier.com/locate/ejmech

Original article

Cationic lipid-conjugated dexamethasone as a selective antitumor agent

Samaresh Sau [a], Rajkumar Banerjee [a, b, *]

[a] Biomaterials Group, CSIR-Indian Institute of Chemical Technology (CSIR-IICT), Tarnaka, Uppal Road, Hyderabad, Andhra Pradesh 500007, India
[b] Academy of Scientific and Innovative Research (AcSIR), 2 Rafi Marg, New Delhi 110 001, India

ARTICLE INFO

Article history:
Received 19 March 2014
Received in revised form
23 June 2014
Accepted 24 June 2014
Available online 25 June 2014

Keywords:
Dexamethasone
Cationic lipid
Glucocorticoid receptor
Apoptosis
Tumor

ABSTRACT

Dexamethasone (Dex) is one of the highly potent synthetic glucocorticoids. It exhibits prominent anti-inflammatory but moderate anti-proliferative activities. It is widely used along side chemotherapy to alleviate toxic side effects. Additionally, Dex is also a potent inducer of gluconeogenesis. However, its overuse critically desensitizes cells against chemotherapy. Herein, we report on the development of a new class of cationic lipid–Dex conjugates in which the C-8 carbon chain analogue (DX8) exhibited glucocorticoid receptor (GR)-mediated, caspase-3-assisted, cancer cell-selective anti-proliferative activity. Melanoma tumors in DX8-treated mice exhibited significantly reduced tumor aggressiveness with respect to tumors in Dex-treated mice. Tumor lysates prepared from DX8-treated group showed elevated levels of p53. DX8-treated cancer cells showed clear degradation of kinase JAK3/STAT3 protein levels. Additionally, DX8-treatment decreased the level of VEGFR2 in tumor-endothelial cells implying DX8's anti-proliferative roles in both tumor cells and tumor neovascular cells. Collectively, our results demonstrate potent anti-angiogenic, and selective JAK3/STAT3 down-regulating anticancer characteristics of DX8, a new dexamethasone-based antitumor molecule.

1. Introduction

Glucocorticoid receptors (GR) are nuclear hormone receptors ubiquitously expressed in both cancer and non-cancer cells. GRs play many crucial roles in various cellular mechanisms. These include cellular energy metabolism involving non-carbohydrate precursors for glucose homeostasis, regulation of protein and fat metabolism and various anti-inflammatory and immunosuppressive responses [1,2]. With structural elucidation of ligand-binding domain (LBD) of GR an upsurge of studies ensued to develop selective GR-ligands. These studies led to better understanding of the conformation of ligand–receptor complexes and thereby the fate & functions of GR [3,4]. These also helped in optimizing ligands' anti-inflammatory activities with reduced side-effect profile.

Classically, glucocorticoids (GC) exert their function by binding to the intracellular GR. Upon ligand-binding GR translocates to the nucleus. Therein, it interacts with specific DNA sequences (popularly known as glucocorticoid response elements, GREs), i.e., with promoter sequences of target genes, resulting in their transcriptional activation [5]. For GR-targeting and transactivation, we chose to use the synthetic GC ligand Dex instead of natural ligand cortisol due to its superior activity in transactivating glucocorticoid responsive genes than cortisol. Additionally, Dex exhibits effective binding with even mutated LBD [6].

Dexamethasone (Dex) is a widely used synthetic GC for inducing apoptotic cell deaths in malignant lymphoid and in other cancer cells [7,8]. In general, these GCs are used in patients during and post-chemotherapeutic treatment of solid tumors to control dehydration, nausea, acute toxicity, edema, and pain towards protecting normal tissues of cancer patients against long-term effects of genotoxic drugs [9]. Dex also exhibits contrasting pharmacological properties. In one hand, Dex exhibits anticancer activity [8]. One of the possible anticancer mechanisms elucidated so far involves the regulation of STAT kinases [10]. On the other hand, Dex induces insensitivity in cancer cells against anticancer drugs [11,12]. So the restricted and carefully regulated use of Dex is needed for effective anticancer treatments.

Previously, we showed that a Dex-associated cationic liposomal gene delivery system could selectively transfect cancerous cells and tumor *in vivo* via GR [13]. This selectivity was observed in spite of

* Corresponding author. Biomaterials Group, CSIR-Indian Institute of Chemical Technology (CSIR-IICT), Tarnaka, Uppal Road, Hyderabad 500007, India.
E-mail addresses: banerjee@iict.res.in, rkbanerjee@yahoo.com, rkbanerjee.iict@gmail.com (R. Banerjee).

http://dx.doi.org/10.1016/j.ejmech.2014.06.051
0223-5234/

GR's ubiquitous presence in both cancer and non-cancer cells. In this liposomal system Dex was associated as a co-lipid with other lipids. We questioned: if, instead of mere association as a co-lipid in a liposome, Dex is conjugated with a cationic lipid will it be able to exhibit selective anticancer effect? To this end, we undertook chemical conjugation of 'cationic, twin carbon chain-length lipid' with Dex. Lipids with cationic head-groups have inherent affinity toward negatively charged cell membranes resulting in enhanced interaction with trans-membrane proteins [14]. Thus, cationic lipid-conjugated Dex is expected to have more availability and local concentration inside the cells than free Dex. We found that this cationic Dex derivative could maintain uncompromised GR-transactivation property of Dex.

Recently we reported that similar cationic lipid-conjugation to estrogen, the natural ligand for estrogen receptor (ER), converted the estrogen molecule into a very potent anti-breast cancer agent. The molecule acts through induction of apoptosis and autophagy in breast cancer cells [15]. The cationic lipid-conjugation also converted haloperidol into a potent anticancer agent [14]. Subsequently, others have also shown the pharmacologic benefit of cationic lipid conjugation to benzamide [16]. These prior studies clearly exemplify that cationic lipid conjugation (or 'lipidation') of known pharmacophores holds promise toward developing new class of drug molecules. On the basis of these recent observations (Scheme 1A), we sought to develop newer cancer targeted molecules through conjugation of cationic lipid to GR ligand, Dex. We hypothesized that the modified Dex-molecule will resurrect programmed cell death machinery against aggressive cancer. Herein we report on the development of a new kind of cationic Dex-derivatives. We show that the lead molecule DX8 exhibited GR-mediated, effective tumor growth inhibition presumably through down-regulation of JAK-STAT pathway with concomitant up-regulation of p53.

2. Results and discussion

2.1. Chemistry

2.1.1. Syntheses of Dex-derivatives

In the present study, we chemically conjugated cationic twin-carbon chain lipid with Dex. Since different Dex derivatives differed by respective lengths of carbon chain linked to quaternary Nitrogen atom, a general procedure was used to synthesize them (Scheme 1B). At first the amino group of *tert*-butyl N-(2-aminoethyl)carbamate was reacted with alkyl bromides of different carbon chain lengths to obtain respective tertiary amines (**1a**–**e**). This was followed by N-deprotection to give free 1^0 amines (**2a**–**2e**). Separately, Dex was oxidized using $NaIO_4$ to produce free carboxylic acid functionality-containing compound **3**, which contains one less carbon than the Dex [17]. The compound **3** was coupled to free 1^0 amine linked to dialkyl amine moiety (**2a**–**2e**) using EDCI/HOBT/DMAP, to produce amide products (**4a**–**4e**). The resulting tertiary amine upon quaternization with methyl iodide followed by chloride ion exchange, afforded pure target lipids (**5a**–**5e**) [DXn, where $n = 2$, 4, 8, 12, and 16 numbers of carbon-containing long chains] (Scheme 1A, B). All Derivatives were characterized using mass and NMR spectrometry (S1–S43). The purities of the respective compounds were determined and confirmed by HPLC (S44–S48).

2.2. Biology

2.2.1. Screening of Dex-derivatives for selective cytotoxicity

For screening the anticancer property of the newly synthesized Dex-derivatives we chose cancer cell lines (B16F10, MCF-7, and A549) and non-cancer cells or cells of primary origin (CHO, HEK293T and mouse skin fibroblast, FB). Both cancer and non-

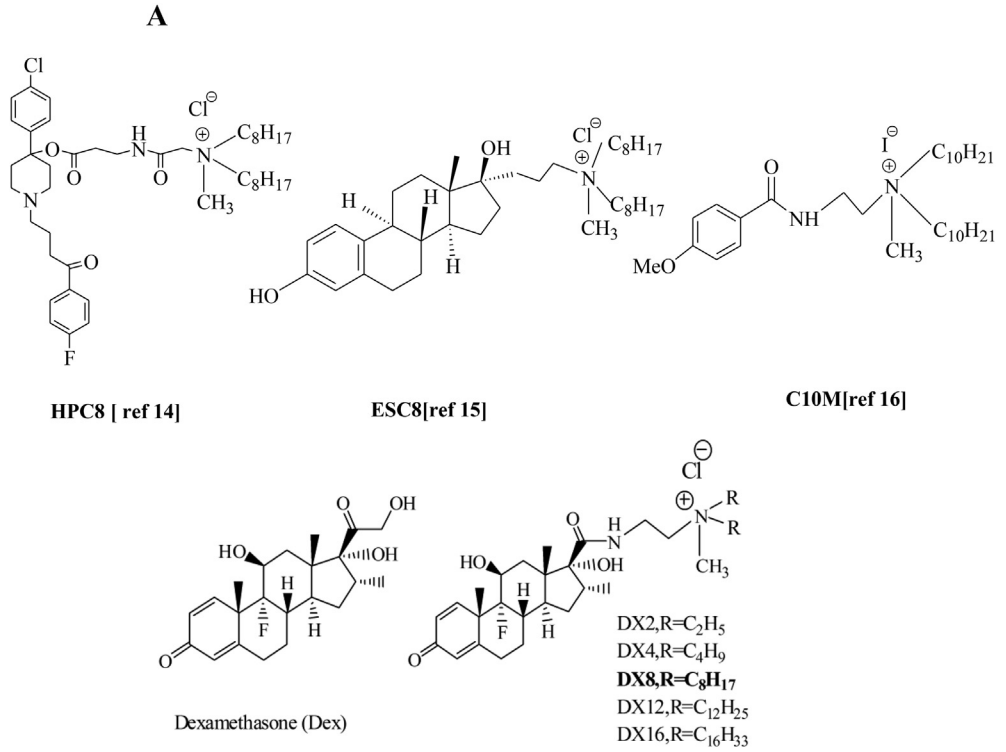

Scheme 1. A: Chemical structures of cationic lipid conjugated anticancer agents, dexamethasone (Dex) and newly synthesized cationic Dex-derivatives. B: syntheses of dexamethasone derivatives.

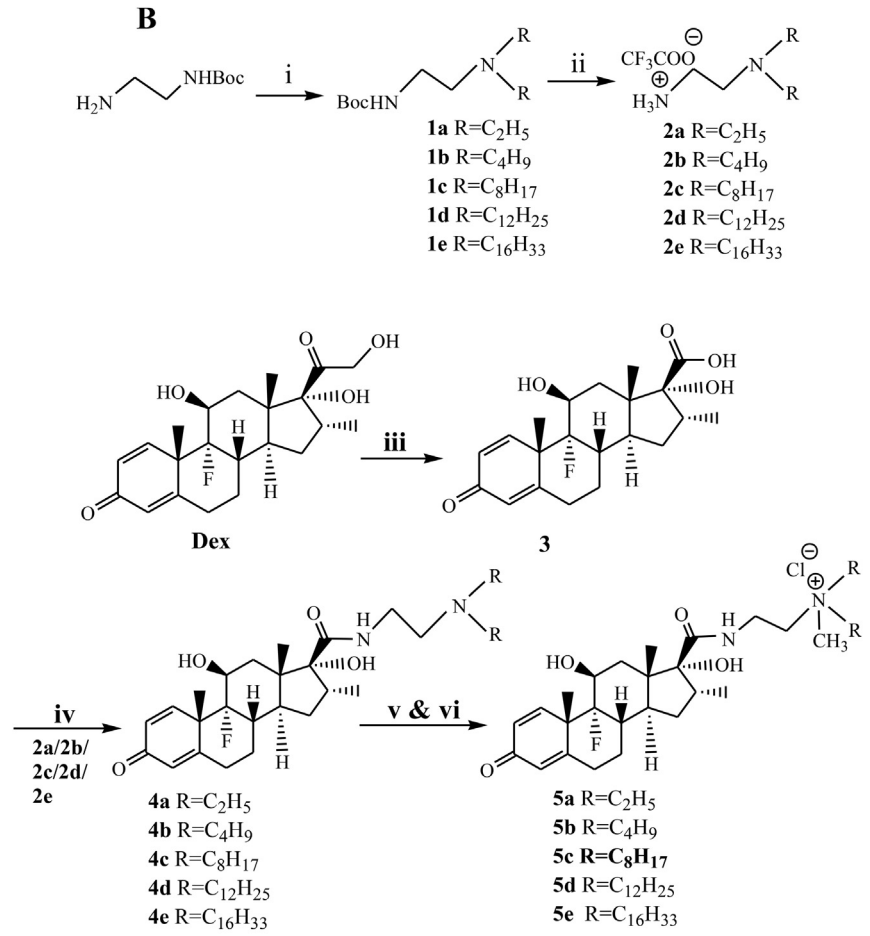

Reagents and conditions:(i) (**i**) R-X (R=alkyl group, X=Br), potassium carbonate (K_2CO_3), ethyl acetate, 70-80 ^{0}C; (**ii**) 50% tri-fluoroacetic acid (TFA) in dichloroethane (DCM); (**iii**) sodium periodate ($NaIO_4$), sulphuric acid (H_2SO_4), water (H_2O), ethanol (EtOH) and overnight stirring; (**iv**) 1-Ethyl-3-(3-dimethylaminopropyl)carbodiimide (EDCI), Hydroxybenzotriazole (HOBt), N, N-diisopropylethylamine (DIPEA), anhydrous DCM and/or dry DMF; (**v**) Methyl Iodide (MeI), anhydrous DCM and K_2CO_3; (**vi**) Amberlite IRA 400Cl, Methanol.

Scheme 1. (*continued*).

cancer cells were treated continuously for 72 h with varying molar concentrations of Dex-derivatives and Dex. Clearly, among the five synthesized Dex-derivatives, DX8 induced maximum toxicity to tested cancer cells (Table 1). The toxicity profiles of DX2, DX4, DX12 and DX16 were more or less comparable to those of free Dex. Keeping 15 μM as threshold IC_{50} for lead screening, we found DX8 to be the most potent anticancer compound among all other derivatives. On the basis of this screening result we undertook mechanistic studies to decipher the cellular and molecular role of DX8 and finally assayed its therapeutic efficiency in tumor model.

Table 1
Anticancer activities (IC_{50}, μM) of Dex and cationic Dex-derivatives in cancer cells (B16F10, MCF-7 and A549) and non-cancer cells (CHO, HEK293T, mouse skin fibroblast cells FB).

Compound IC_{50} (μM)	B16F10	MCF7	A549	CHO	HEK293T	FB
Dex	>20	>15	>15	>20	>20	>15
DX2	>20	>15	>15	>15	>20	>20
DX4	>20	>15	>15	>20	>15	>20
DX8	6.0 ± 0.68	6.5 ± 0.42	7.2 ± 0.54	>15	>15	>15
DX12	>15	13.5 ± 0.46	14.0 ± 0.7	>20	>15	>15
DX16	>15	>15	14.8 ± 0.53	>15	>20	>15

2.2.2. DX8 is more toxic to cancer cells than normal cells

GRs are ubiquitously expressed in all type of cancerous and non-cancerous cells. So, it was necessary to assess DX8's selectivity (if any) in killing cancer cells. We also compared DX8's cellular effect to that of parent molecule Dex. On the basis of data represented in Table 1 we further demonstrate the cellular effect of DX8 and Dex against cancer cells (B16F10, MCF-7, and A549) and non-cancer cells (CHO, HEK293T and mouse skin fibroblast, FB) (Fig. 1a). Clearly, DX8 exhibited significantly higher toxicity than free Dex in cancer cells. But, DX8-induced toxicity was insignificant against non-cancer cells. Notably, unconjugated cationic C8-lipid component (i.e., cationic C8-side chain) exhibited some but significantly lesser cytotoxicity against various cancer cells than that exhibited by DX8 (data not shown) [We have also demonstrated this limited cellular toxicity effect of C8-lipid component independently in Ref. [14]]. Overall, these findings demonstrate DX8's selective cytotoxicity in cancer cells thereby validating the need to conjugate cationic lipid moiety to Dex.

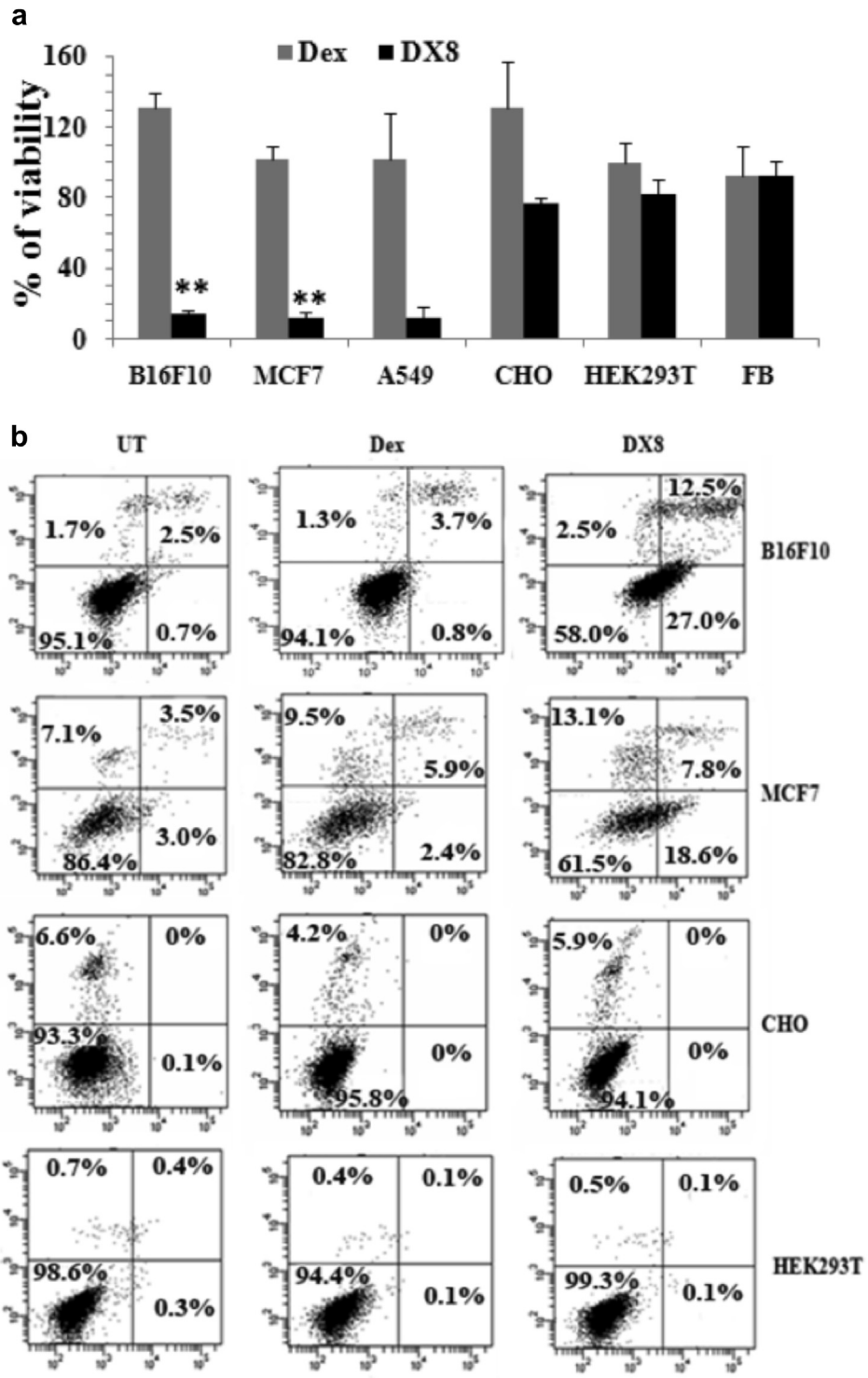

Fig. 1. Cytotoxic and apoptosis inducing effect on cancer and non-cancer cells. (a) Viability studies of B16F10, MCF7, A549 (cancer cells) and CHO, HEK293T, mouse skin fibroblast or FB (non-cancer cells) continuously treated with Dex and DX8 for 72 h. The asterisks (**) denote $p < 0.001$ for DX8 with respect Dex. (b) Flow cytometric analysis of apoptosis in B16F10, MCF-7, CHO and HEK293T cells co-stained with FITC-annexin V/propidium iodide (PI). The horizontal and vertical axes represent FITC-annexin V and PI staining, respectively. Cells were either untreated or treated with 10 μM Dex, DX8 for continuously 48 h.

2.2.3. DX8 induces apoptosis in cancer cells but not in normal cells

Apoptosis inducing effect of the DX8 was determined by conventional propidium iodide (PI)/annexin V binding assay. The initial events of apoptosis indicate loss of plasma membrane integrity. Thereafter, phosphatidylserine (PS) translocates from the inner to outer membrane leaflets, thereby exposing itself to external environment. Annexin V with high affinity for PS binds to cells efficiently with externally exposed PS. Thus, more the positive staining of fluorescently labeled annexin V more is the loss of cell membrane polarity. This precedes complete loss of membrane integrity accompanying the later stage of cell death resulting from either apoptosis or necrosis. On the contrary, PI can only enter into

cells after loss of membrane integrity. Dual stain with annexin V and PI thus allows obvious discrimination among unaffected cells (annexin V negative, PI negative, lower left quadrant), early apoptotic cells (annexin V positive, PI negative, lower right quadrant), late apoptotic cells (annexin V positive, PI positive, upper right quadrant), and necrotic cells (annexin V negative, PI positive, upper left quadrant). As indicated, for early apoptotic cells an elevated amount of annexin V stained cells is expected in lower right quadrant. To observe selective induction of cellular apoptosis (if any), we chose four cell lines B16F10, MCF-7 (all cancer cells) and CHO, HEK293T (non-cancer cells). Fig. 1b shows that DX8 treatment (10 μM, for 48 h) increased the percentage of early apoptotic cells (with annexin V positive and PI negative staining, lower right quadrant) in only cancer. Contrastingly, Dex (10 μM, for 48 h) induced such effect neither in cancer nor in non-cancer cells. Therefore, this is obvious that DX8 at the given condition of treatment selectively induced early signs of apoptosis in cancer cells, but not in non-cancer cells.

2.2.4. *DX8 induces GR-mediated toxicity in cancer cells*

For this study, we used siRNA-based silencing strategy to knock down effective GR concentration in B16F10 and A549 cancer cells. In this experiment, we pre-transfected cells separately with siRNA against GR (GR-siRNA), and with control universally scrambled siRNA (Sc-siRNA). Group, wherein cells were not treated with siRNA was used as untreated (UT) control. Cells were treated with DX8 and DX8-induced toxicities in different groups were compared. Flow cytometric analyses of B16F10 (Fig. 2a) and A549 (Fig. 2c) cells clearly show that there were lesser levels of GR in GR-siRNA treated cells than those in Sc-siRNA treated or UT cells. Cellular viability trend reveals that DX8-mediated toxicity in GR-depleted (i.e., GR-siRNA pre-transfected) B16F10 (Fig. 2b) and A549 (Fig. 2d) cells were significantly lower than that in Sc-siRNA-treated or UT cells. Additionally, we also observed reversal of DX8-mediated toxicity in RU 486-pretreated B16F10 cells (data not shown). RU-486 is a known GR-antagonist. Notably, the decrease in DX8-induced toxicity in GR-depleted cells was significant. This data clearly suggests that the DX8-induced toxicity was GR-mediated. In other words, DX8-mediated toxicity in cancer cells was GR-dependent.

2.2.5. *Tumor growth inhibition & anti-angiogenic properties of DX8*

DX8 was the lead molecule among all the derivatives. Hence, we wanted to see its *in vivo* therapeutic effect in a tumor model. For an *in vivo* tumor regression study we used highly aggressive B16F10-based murine melanoma model in C57BL6/J black mice. Moreover, in this model, the aggressive tumor develops high levels of angiogenic blood vessels and hence any treatment-related effect on angiogenesis can be additionally documented. By flow cytometric analyses we showed that DX8 induces prominent, early signs of apoptosis in B16F10 cells. Hence, DX8 was administered in mice to estimate its tumor regression efficacy and its tumor regression property was compared to that of Dex. After the completion of the experimentation, tumors from individual groups were cryosectioned for imaging apoptotic signs (if any) using green fluorescent TUNEL (Terminal deoxynucleotidyl transferase dUTP nick end labeling) assay kit and using VE-cadherin antibody (red fluorescence) as angiogenic blood vessels. Fig. 3a shows that DX8-treatment significantly inhibited tumor growth, especially with respect to tumor growths in Dex-treated mice and in untreated (UT) groups. Fig. 3b exhibits the images of representative tumors excised from sacrificed mice from individual groups at the completion of treatment. Fig. 3c indicates the images of apoptotic regions (green fluorescence) and blood endothelial cell-associated sites (red fluorescence) obtained from tumor sections of different treatment groups. Merged images of sections are also shown. Here, 'yellow' areas (merging of green and red areas) denote sites where vascular endothelial cells underwent apoptosis. Evidently, tumor sections from DX8-treated group contain more apoptotic regions than in tumor sections from the

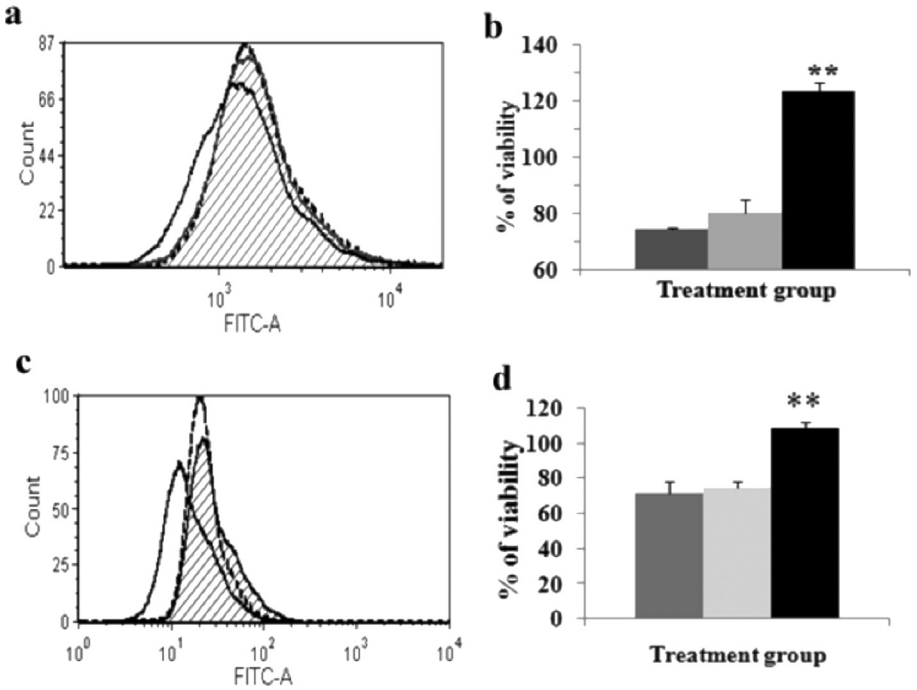

Fig. 2. Effect of GR down-regulation in DX8-mediated cytotoxicity in cancer cells. Flow cytometric analysis of GR down-regulation in (a) B16F10 and (c) A549 cell lines. Black line, dashed line and striped area represent, GR levels in GR-siRNA treated, negative control siRNA treated, and siRNA untreated cells respectively. Viability test in (b) B16F10 and (d) A549 cells and correspondingly the dark gray (■), light gray (■) and black (■) bars represent siRNA-untreated (UT), scrambled control siRNA-treated, GR-siRNA treated cells. ** denotes $p < 0.001$ for GR-siRNA treated vs. control siRNA-treated groups.

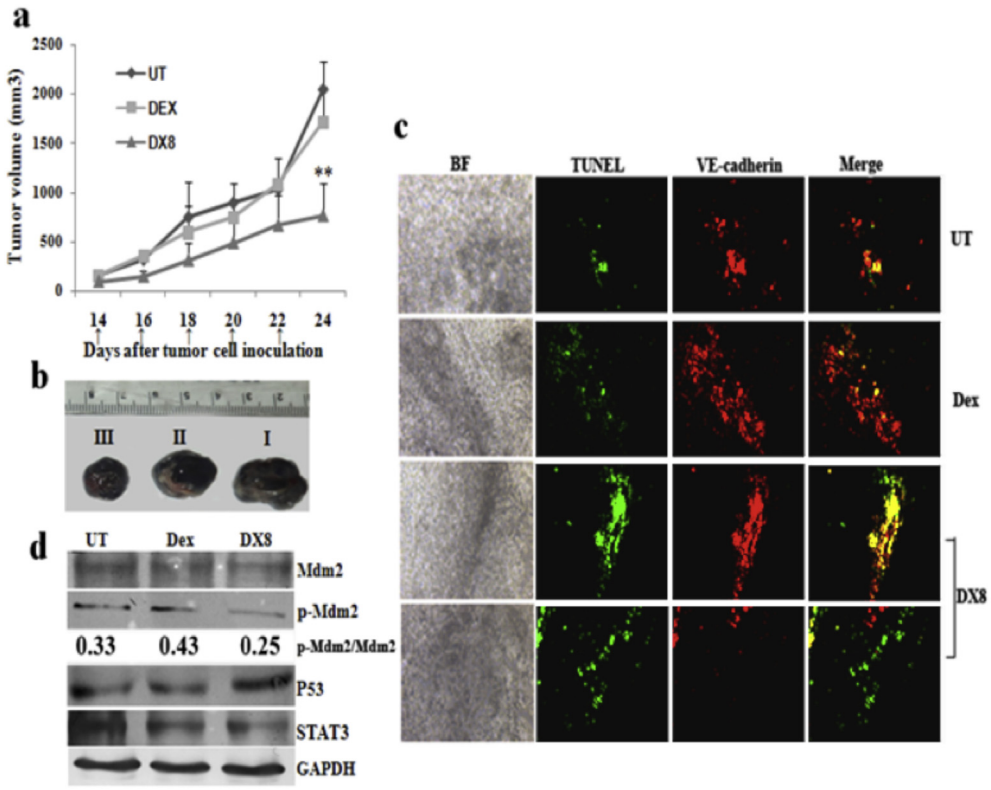

Fig. 3. *In vivo* effect of DX8. (a) Tumor regression curve after subcutaneous implantation of B16F10 cells in C57BL6/J mice followed by intraperitoneal injection of Dex, DX8 or kept untreated (UT). The days of injections are indicated by black arrows. ** denotes $p < 0.05$ for DX8 treatment with respect to Dex treatment. (b) Representative tumors from sacrificed mice on day 24th; (**I**) tumor from untreated group (UT), (**II**) tumor from Dex-treated group, (**III**) tumor from DX8-treated group. (c) Microscopic pictures of 10 μm tumor sections from UT (upper panel), Dex (middle panel) and DX8 treated group (lower panel). Left column indicates tissue architecture in bright field (BF), next from left column shows apoptotic regions in TUNEL assay (green fluorescent), second from right column exhibits endothelial region stained with VE-cadherin (red fluorescent) and extreme right panel exhibits merged green and red fluorescent images of middle columns respectively. All the images are taken at 10× magnification. (d) Western blot analysis of tumor lysates isolated from UT, Dex and DX8-treated mice group. (For interpretation of the references to color in this figure legend, the reader is referred to the web version of this article.)

Dex or UT groups. Clearly, DX8 could induce significant apoptosis in cultured cancer cells and also, as depicted here, in highly aggressive melanoma tumor tissues. Illustratively, tumor sections of DX8-treated group exhibit considerable amount of apoptosis in cells prevailing in tumor microenvironment. This apoptotic effect could have resulted in significant inhibition of tumor growth. Using VE-cadherin staining for blood vessels in tumor sections, we found that tumor sections of DX8-treated group exhibit very high levels of apoptosis in vascular endothelial cells also (when compared to the yellow areas in merged panels). These data together indicate that the significant tumor-regression in DX8-treated group could be due to simultaneous apoptosis in both vascular endothelial cells as well as in tumor cells of tumor mass. For DX8-treated group, we have provided two sets of tumor section panels representing two different areas with different levels of vascular cells in tumor sections.

p53 protein is a key regulator of apoptosis mediated cell death, DNA repair and senescence. The inactivation of p53 increases the threat of cancer. The mechanism of p53 inactivation is however a complex process. Typically, inactivation of p53 occurs because of activation of Mdm2 (i.e., preferable conversion to p-Mdm2), which negatively regulates p53 stability and regulation [18]. Fig. 3d exhibits the relative expression of Mdm2, p-Mdm2, and p53 proteins in tumor lysates from different treatment groups. Importantly, significant up-regulation of p53 and down-regulation of p-Mdm2 in tumor lysates from DX8-treated group were observed. These indicate that DX8-treatment could have affected inhibition of Mdm2 phosphorylation thereby impeding sequestration of p53-activation in aggressive tumor mass.

2.2.6. DX8 down-regulates VEGFR2 expression in tumor-associated angiogenic cells

Tyrosine kinase VEGFR2 is one of the important factors that have been implicated in tumor angiogenesis and aggression. Following VEGF-binding it activates and regulates endothelial blood vessel formation, survival and activation of downstream kinases, such as Akt [19]. From Fig. 3a–b it is clear that DX8, in comparison to Dex, was more potent in inducing tumor growth inhibition presumably due to enhanced apoptosis in tumor-associated endothelial cells. We hypothesized that reduction in tumor aggression was linked to down-regulation of the pro-angiogenic factor, VEGFR2. To visualize this effect, we co-stained VEGFR2 (with green fluorescent secondary antibody) and endothelial cell junction protein, VE-cadherin (with red fluorescent secondary antibody) in tumor sections. The ratio of VEGFR2 expression to that of stained endothelial cells was minimum in tumor sections of DX8-treated group. The ratio was comparatively higher in tumor sections of Dex-treated and UT mice (Fig. 4). This comparative loss of potent receptor VEGFR2 on angiogenic vessels should be expected to eventually reduce angiogenesis in tumors of DX8-treated group. The reason for this incidental reduction in VEGFR2 expression level in DX8-treated group is currently not known. However, we believe that the

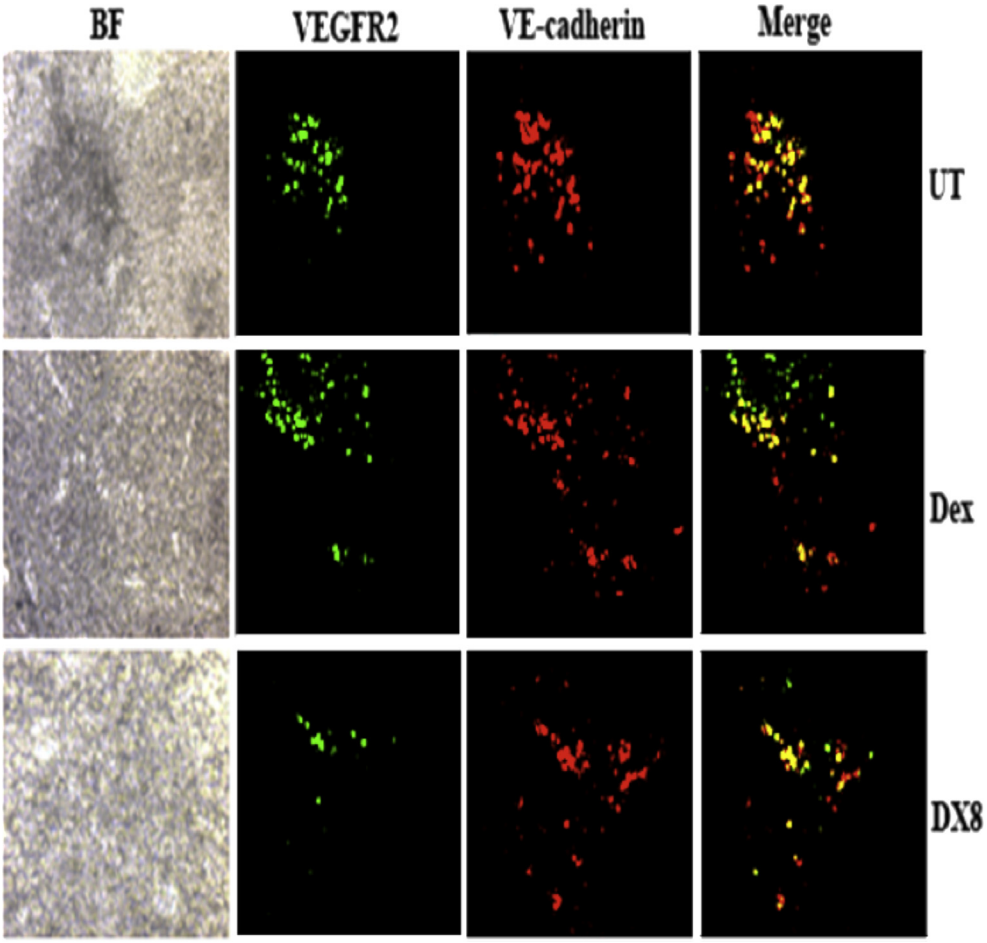

Fig. 4. Effect of DX8 on VEGFR2. VEGFR2 down-regulation in tumor section either from Dex (middle panel), DX8 (lower panel) treated mice or UT (upper panel). From left first column respectively indicates the tissue architecture in bright field (BF), second column represents VEGFR2 staining (green fluorescent), third panel represents endothelial region stained with VE-cadherin (red fluorescent) and extreme right as merged images of middle panels. (For interpretation of the references to color in this figure legend, the reader is referred to the web version of this article.)

effective reduction in VEGFR2 was eventually linked to significant reduction in tumor aggressiveness.

2.2.7. DX8 triggers apoptosis in B16F10 cells

The B16F10 cell-based murine melanoma model was chosen for *in vivo* study (Fig. 3). Hence, the mechanism of DX8-mediated toxicity was determined in B16F10 cells. B16F10 cells were either treated with DX8, Dex or kept untreated (UT) for 48 h. This was done to elucidate how DX8 could have affected various cancer-implicated factors in these cells before inducing prominent cell killing after 72 h. During apoptosis, mitochondria releases cytochrome-c in cytosol. Eventually, this activates caspase family of proteases. Activation of caspase 9 by cytochrome c cleaves procaspase 3 to release effector caspase i.e., activated caspase 3 [20]. The release of caspase 3 leads to induction of apoptosis in cells. However, Bcl-2 family of proteins regulate the mitochondrial release of cytochrome c [21]. A member of this family, such as BAX (Bcl-2-associated X protein) causes the release of cytochrome c and thus initiate apoptosis. On the other hand anti-apoptotic members of this family, such as Bcl-2 bind to the pro-apoptotic BAX protein and inhibit release of cytochrome c. So a higher value of BAX/Bcl-2 ratio indicates the onset of apoptosis in cells. As seen in Fig. 5a, the ratio of BAX/Bcl-2 expression in DX8-treated cells was higher than in Dex-treated or in UT cells. An elevated expression of caspase 9 and elevated proteolytic cleavage of caspase 3 to form activated caspase 3 were also observed in DX8-treated cells. Additionally, selective up-regulation of caspase 7 was also observed in DX8-treated cells. These sequential events possibly triggered the pathway of apoptosis, which led to a) high level of cytotoxicity in B16F10 cells (as observed in Fig. 1a), b) increased population of early apoptotic cells as shown in Annexin V/PI experiment (Fig. 1b and c) apoptotic lesions in tumor sections as shown in TUNEL data (Fig. 3c).

The 'X-linked inhibitors of apoptosis' (XIAP) inhibits and helps proteolytic degradation of effector caspase-3. This process is however antagonized by Smac [22]. Fig. 5b shows that DX8 released mitochondria derived activator (Smac/Diablo) and inhibited the expression of XIAP, which possibly led to stabilization of activated caspase-3. It seems, DX8-induced apoptosis in cancer cells was causally linked to caspase-induced apoptotic pathway. This was sequentially revealed by increase in the ratio of BAX/Bcl-2, which led to the release of cytochrome c. These we believe prominently increased fragmented (or activated) caspase 3. The stabilization of fragmented caspase-3 is also related to down-regulation of anti-apoptotic factor, XIAP and up-regulation of pro-apoptotic factor, Smac/Diablo [23]. Thus, the increased levels of pro-apoptotic factor Smac/Diablo and decreased levels of anti-apoptotic factor XIAP were possibly responsible for DX8-induced apoptosis in B16F10 cells.

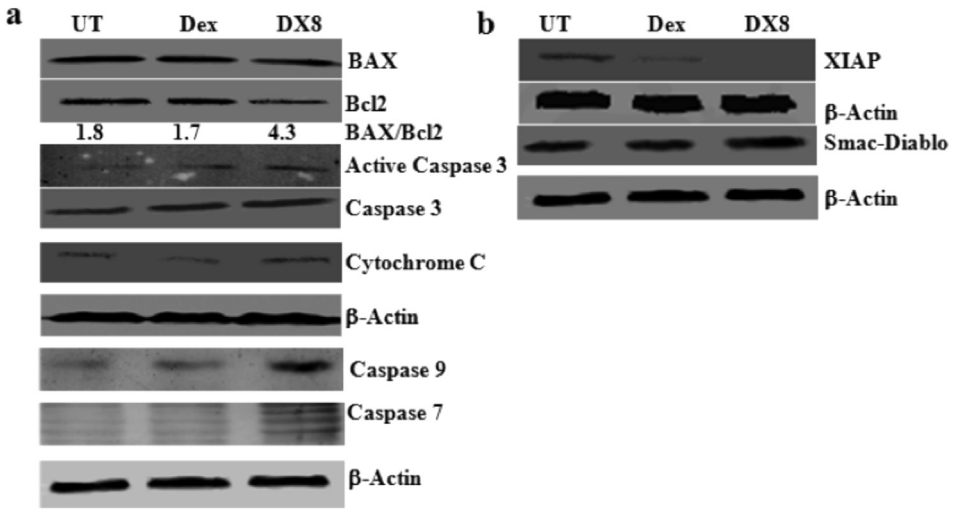

Fig. 5. Differential expression of different regulators of apoptosis and proliferation in compound-treated B16F10 cells. Cells were either treated with Dex (10 μM) and DX8 (10 μM) or kept untreated (UT) for 48 h (a) Western blots of apoptosis related proteins such as, BAX, Bcl2, Active Caspase 3, Caspase 3, cytochrome c, Caspase 9 and 7 and loading control β-actin are presented. The densitometric ratio of BAX and Bcl2 is determined using 'Image J' software. (b) Similarly, respective levels of expression of XIAP and Smac-Diablo with respect to loading control β-actin were estimated.

2.2.8. Role of Akt and activation of p53 through JAK/STAT3 pathway

Akt has leading role in tumorigenesis. It crucially acts among numerous signaling cascades involved in the regulation of cellular apoptosis and proliferation [24,25]. Further, Tyrosine-kinases such as, janus kinases (JAK) are also involved in activation of Akt through JAK/STAT pathway in cell survival machinery [26]. Pro-apoptotic factor p53 is a potent inhibitor of cell growth. It regulates cell cycle progression at several check-points and induces apoptosis to control cell proliferation and cell division [27,28]. In tumors from DX8-treated group, p53 up-regulation was observed. Here we tried to understand whether the induction of apoptosis at a cellular level was due to reactivation of p53. P53-up regulation occurs because of downregulation of p-Mdm2. Phosphorylation of Akt leads to nucleo-cytoplasmic localization of vital substrates implicated in cell cycle and apoptosis. In presence of growth factor, p-Akt phosphorylates Mdm2, which then enters nucleus. Nuclear translocation of p-Mdm2 leads to the formation of Mdm2–p53 complexes, which allows phosphorylation of p53 and its relocation to the cytoplasm for subsequent ubiquitination and degradation [18,28]. The oncoprotein Mdm2 and the tumor suppressor p53 are part of this auto-regulatory feedback. As we can see from Fig. 6a, in DX8 treated B16F10 cells JAK3/STAT3 kinases were significantly down-regulated which naturally resulted in the reduction of p-STAT3 levels. This DX8-mediated STAT3 down-regulation possibly antagonized p-Akt formation/stabilization; this eventually led to Akt's destruction (Fig. 6b). We believe Akt's destruction eventually inhibited phosphorylation of Mdm2 (shown in tumor mass, Fig. 3d), resulting in its possibly restricted nuclear interaction with p53. Hence, level of p53 was up-regulated in DX8-treated cancer cells (Fig. 6c).

The data as obtained by the treatment of DX8 to cancer cells and in tumor model revealed that the lipid-modification enhances or value-adds the existing, known pharmacologic effects of GR ligand, Dex. The well-known GR ligand Dex reduces NF-kB-mediated anti-proliferation or inflammatory syndromes. It is co-treated to cancer patients during chemotherapy. This is done to alleviate various inflammatory side effects of drug treatment. However, it is also now clear that its widespread use leads to desensitization of target cells during drug-based medical treatment [11,12]. Hence, it was a challenge to chemically modify Dex to make it more potent anticancer agent while possibly overshadowing its desensitizing effects. This study has hence established that cationic lipid modification of Dex clearly afforded a potent anticancer agent.

3. Conclusion

We have modified Dex with cationic lipid and developed a highly selective anticancer agent called DX8, which exhibited therapeutic anticancer potency significantly better than the parent molecule, Dex. Clearly, DX8 showed its pharmacological property preferentially through modulation of JAK3/STAT3 pathway. This data shows that cationic lipid-conjugation to Dex could make a novel class of anticancer agent. Further studies are in progress toward elucidating any drug sensitizing effect of this molecule to cancer cells, which we believe will be an added advantage while developing this new class of anticancer agent. We are also looking into whether or not DX8 exhibits synergism with inhibitors acting downstream of JAK/STAT pathway. To conclude, the strategy adopted herein is expected to find future application in enhancing pharmacological properties and anticancer activities of existing glucocorticoids.

4. Experimental section

4.1. Chemicals and general procedures for characterizations

Dexamethasone (Dex), trypsin, EDTA, 3-(4,5-dimethylthiazol-2-yl)-2,5-diphenyltetrazoliumbromide (MTT), propidium iodide (PI), FITC-labeled annexin V, dimethyl sulfoxide (DMSO), Dulbecco's Modified Eagle Medium (DMEM) and RPMI 1640 were purchased from Sigma Chemical Co. (St. Louis, MO). Fetal bovine serum (FBS) was purchased from Lonza, Swiss chemicals. RU486 purchased from Calbiochem, Merck, USA. Si-RNAs were purchased from Santa Cruz biotechnology, USA. The solvents, salts and common reagents for synthesis were purchased from either Aldrich (Milwaukee, WI, USA) or S. D. Fine Chem (Mumbai, India). All other chemicals, reagents were purchased either from Sigma (St. Louis, MO, USA) or from Rankem Ltd. (Mumbai, India). They were used without further purification. Lipofectamine 2000 was obtained from Invitrogen Corporation (Carlsbad, CA). All other materials for Western blotting

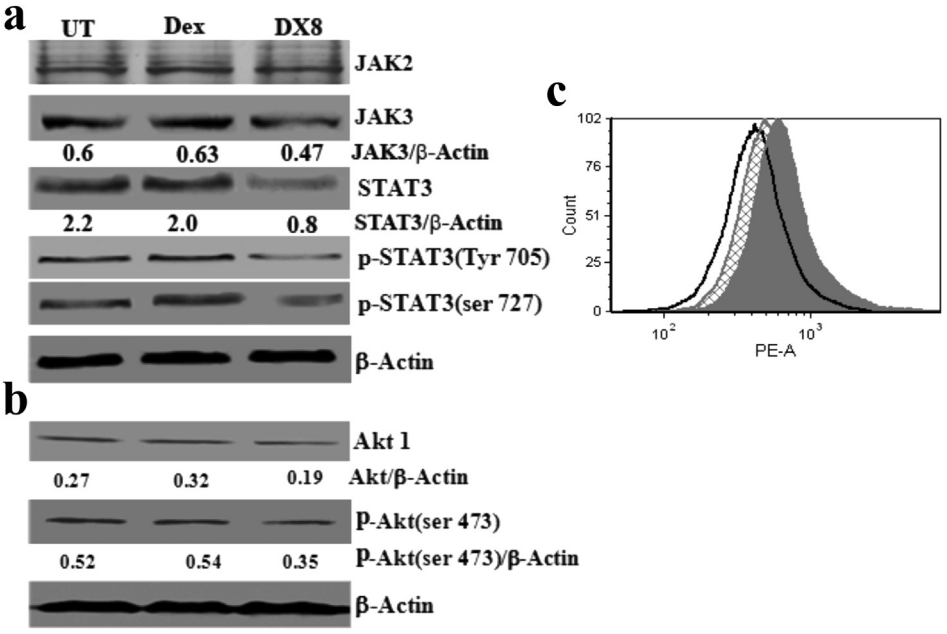

Fig. 6. Western blot analysis of different signaling kinases in compound-treated B16F10 cells. Cells were either treated with 10 μM of Dex and DX8 or kept untreated (UT) for 48 h. (a) Western blots of kinases such as, JAK2, JAK3, STAT3, p-STAT3 (Tyr 705), p-STAT3 (ser 727) and β-actin are presented. Ratios of JAK3/β-actin and STAT3/β-actin are mentioned (b) AKT 1 and p-AKT (ser 473) and the ratio of both with respect to β-actin are determined. (c) Flow cytometric analysis of p53 up-regulation in B16F10 cell line treated after 48 h of treatment. Black line, striped area, and gray area represent levels of p53 in cells from UT, Dex and DX8-treated cells respectively.

were purchased from local company. The final molecules were characterized by ^{1}H NMR and ESI-HRMS spectral analyses and the purity was ascertained by HPLC. ^{1}H NMR spectra were recorded on Varian FT 200 MHz or Bruker FT 300 and 400 MHz spectrometer. ^{13}C NMR was obtained in Bruker FT 75 or 125 MHz. ESI Mass spectra were obtained by Micromass Quattro LC mass spectrometer. Purity of final products was determined in Varian ProStar HPLC at 210 nm at a flow rate of 1 mL/min in Varian microsorb 100-10 BDS column (4.6 mm × 250 mm); Mobile Phase: For DX2 (Methanol), for DX4 (Acetonitrile), DX8 (Methanol), DX12 (95% Methanol–Water system), DX16 (95% Methanol–Water system); Flow Rate: 1 mL/min; Column Pressure: 55–60 kg/cm^2; Temperature: 25 °C; Wavelength: 210 nm.

*4.1.1. Synthesis of tert-butyl N-[2-dialkylamino)ethyl] carbamate, compounds **1a**–**e***

The general syntheses of compounds **1a**–**e** are accomplished by conventional chemical synthesis procedure as described below.

*4.1.1.1. Synthesis of tert-butyl N-[2-(diethylamino)ethyl]carbamate, compound **1a**.* *tert*-Butyl-N-(2-aminoethyl)carbamate (1 g, 6.25 mmol), potassium carbonate (3.45 g, 25 mmol) and 1-bromoethane (1.92 g, 15.62 mmol) were added in 15 mL dry ethyl acetate in a 50 mL round-bottom flask fitted with reflux condenser. The resulting mixture was refluxed over an oil bath at 70–80 °C for 48 h. Then the mixture was cooled, excess ethyl acetate was removed by rotary evaporation and 50 mL chloroform was added into this. The whole mixture was transferred to a 500 mL separating funnel and mixture was washed with water (3 × 100 mL) followed by brine (3 × 100 mL), dried with anhydrous sodium sulfate (Na_2SO_4) and evaporated. The resulting solution was purified by column chromatography using 60–120 mesh silica gel and 7% ethyl acetate–hexane (v/v) as eluent. This yielded compound **1a** as a yellowish liquid (0.74 g, 55% yield, R_f = 0.5 in 30% ethyl acetate–hexane, v/v).

^{1}H NMR (400 MHz, $CDCl_3$): δ/ppm = 0.94–1.01 [t, J = 7.3 Hz, 6H, $-N(-CH_2-C\boldsymbol{H}_3)_2$], 1.36 [s, 9H, $-NH-CO-O-C(C\boldsymbol{H}_3)_3$], 2.46–2.56 [m, 6H, $-N(-C\boldsymbol{H}_2-CH_3)_2$, $-C\boldsymbol{H}_2-CH_2-NH-CO-O-C(CH_3)_3$], 3.10–3.17 [m, 2H, $-CH_2-C\boldsymbol{H}_2-NH-CO-O-C(CH_3)_3$].

ESI–MS: m/z 217 (Calculated value for $C_{11}H_{24}N_2O_2$ = 216.3).

*4.1.1.2. Synthesis of tert-butyl N-[2-(dibutylamino)ethyl]carbamate, compound **1b**.* *tert*-Butyl-N-[2-(dibutylamino)ethyl]carbamate, **1b** was synthesized following a similar procedure as described for **1a** synthesis above. Here 1-bromobutane was used. (Compound **1b**: 1.11 g, 65.2% yield, R_f = 0.55 in 30% ethyl acetate–hexane, v/v).

^{1}H NMR (300 MHz, $CDCl_3$): δ/ppm = 0.83–0.89 [t, J = 7.9 Hz, 6H, $-N(-CH_2-CH_2-CH_2-C\boldsymbol{H}_3)_2$], 1.17–1.28 [m, 4H, $-N(-CH_2-CH_2-C\boldsymbol{H}_2-CH_3)_2$], 1.37–1.45 [m, 13H, $-NH-CO-O-C(C\boldsymbol{H}_3)_3$, $-N(-CH_2-C\boldsymbol{H}_2-CH_2-CH_3)_2$], 2.35–2.42 [t, J = 6.9 Hz, 4H,$-N(-C\boldsymbol{H}_2-CH_2-CH_2-CH_3)_2$], 2.45–2.51 [t, J = 6.9 Hz, 2H, $-C\boldsymbol{H}_2-CH_2-NH-CO-O-C(CH_3)_3$], 3.03–3.31 [m, 2H, $-CH_2-C\boldsymbol{H}_2-NH-CO-O-C(CH_3)_3$], 5.03 [s, 1H].

ESI–MS: m/z 273 (Calculated value for $C_{15}H_{32}N_2O_2$ = 272.4).

*4.1.1.3. Synthesis of tert-butyl N-[2-(dioctylamino)ethyl]carbamate, compound **1c**.* *tert*-Butyl-N-[2-(dioctylamino)ethyl]carbamate, **1c** was synthesized following a similar procedure as described for **1a** synthesis. Here 1-bromooctane was used. (Compound **1c**: 1.70 g, 70.0% yield, R_f = 0.6 in 30% ethyl acetate–hexane, v/v).

^{1}H NMR (400 MHz, $CDCl_3$): δ/ppm = 0.82–0.92 [t, J = 7.7 Hz, 6H, $-N(-CH_2-CH_2-(CH_2)_5-C\boldsymbol{H}_3)_2$], 1.11–1.33 [m, 20H, $-N(-CH_2-CH_2-(C\boldsymbol{H}_2)_5-CH_3)_2$], 1.43–1.50 [m, 13H, $-NH-CO-O-C(C\boldsymbol{H}_3)_3$, $-N(-CH_2-C\boldsymbol{H}_2-(CH_2)_5-CH_3)_2$], 2.34–2.43 [t, J = 6.9 Hz, 4H, $-N(-C\boldsymbol{H}_2-CH_2-(CH_2)_5-CH_3)_2$], 2.46–2.52 [t, J = 5.8 Hz, 2H,$-C\boldsymbol{H}_2-CH_2-NH-CO-O-C(CH_3)_3$], 3.07–3.17 [m, 2H, $-CH_2-C\boldsymbol{H}_2-NH-CO-O-C(CH_3)_3$], 7.32 [s, 1H, $CDCl_3$].

ESI–MS: m/z 385 (Calculated value for $C_{23}H_{48}N_2O_2$ = 384.6).

*4.1.1.4. Synthesis of tert-butyl N-[2-(didodecylamino) ethyl]carbamate, compound **1d**.*

tert-Butyl-N-[2-(didodecylamino)ethyl]carbamate, **1d** was synthesized following a similar procedure as described for **1a** synthesis.

Here 1-bromododecane was used. (Compound **1d**: 2.09 g, 67.0% yield, $R_f = 0.7$ in 30% Ethyl acetate–hexane, v/v).

^{1}H NMR (300 MHz, $CDCl_3$): δ/ppm = 0.83–0.89 [t, J = 7.1 Hz, 6H, $-N(-CH_2-CH_2-(CH_2)_9-C\boldsymbol{H}_3)_2$], 1.17–1.34 [m, 36H, $-N(-CH_2-CH_2-(C\boldsymbol{H}_2)_9-CH_3)_2$], 1.42–1.48 [m, 13H, $-NH-CO-O-C(C\boldsymbol{H}_3)_3$, $-N(-CH_2-C\boldsymbol{H}_2-(CH_2)_9-CH_3)_2$], 2.39–2.46 [t, J = 6.4 Hz, 4H, $-N(-C\boldsymbol{H}_2-CH_2-(CH_2)_9-CH_3)_2$], 2.51–2.55 [t, J = 6.0 Hz, 2H, $-C\boldsymbol{H}_2-CH_2-NH-CO-O-C(CH_3)_3$], 2.87–2.90 [m, 2H, $-CH_2-C\boldsymbol{H}_2-NH-CO-O-C(CH_3)_3$].

ESI–MS: m/z 497 (Calculated value for $C_{31}H_{64}N_2O_2 = 496.8$).

*4.1.1.5. Synthesis of tert-butyl N-[2-(dihexadecylamino)ethyl]carbamate, compound **1e**.* *tert*-Butyl-N-[2-(dihexadecylamino) ethyl] carbamate, **1e** was synthesized following a similar procedure as described for **1a** synthesis. Here 1-bromohexadecane was used. (Compound **1e**: 2.31 g, 60.0% yield, Rf = 0.75–0.8 in 30% Ethyl acetate–hexane, v/v).

^{1}H NMR (400 MHz, $CDCl_3$): δ/ppm = 0.81–0.93 [t, J = 6.9 Hz, 6H, $-N(-CH_2-CH_2-(CH_2)_{13}-C\boldsymbol{H}_3)_2$], 1.07–1.35 [m, 52H, $-N(-CH_2-CH_2-(C\boldsymbol{H}_2)_{13}-CH_3)_2$], 1.43–1.47 [m, 13H, $-NH-CO-O-C(C\boldsymbol{H}_3)_3$, $-N(-CH_2-C\boldsymbol{H}_2-(CH_2)_{13}-CH_3)_2$], 2.33–2.44 [t, J = 6.4 Hz, 4H, $-N(-C\boldsymbol{H}_2-CH_2-(CH_2)_{13}-CH_3)_2$], 2.46–2.55 [t, J = 5.8 Hz, 2H, $-C\boldsymbol{H}_2-CH_2-NH-CO-O-C(CH_3)_3$], 3.06–3.22 [m, 2H, $-CH_2-C\boldsymbol{H}_2-NH-CO-O-C(CH_3)_3$], 7.32 [s, 1H, $CDCl_3$].

ESI–MS: m/z 610 (Calculated value for $C_{39}H_{80}N_2O_2 = 609.0$).

*4.1.2. Synthesis of tert[2-(dialkylamino)ethyl]ammonium trifluoroacetate (**2a**–**e**)*

General procedure for Boc-deprotection was followed as described below.

*4.1.2.1. Synthesis of tert[2-(diethylamino)ethyl]ammonium trifluoroacetate, compound **2a**.* Compound **1a** (0.124 g, 0.57 mmol) was dissolved in 4 mL of dry DCM in a 25 mL round-bottom flask and stirred over an ice bath for 15 min. Then 2 mL of trifluoroacetic acid (TFA) was added drop-wise to the solution and stirring was continued for another 4 h over an ice bath. Then the resulting mixture was diluted with chloroform. Excess TFA was removed by washing with saturated sodium bicarbonate ($NaHCO_3$) solution (2 × 50 mL). The organic layer was dried with anhydrous sodium sulfate (Na_2SO_4) and evaporation of the organic layer afforded compound **2a** as a reddish gummy liquid (0.062 g, 93.9% yield, $R_f = 0.1$, active in ninhydrin charring). As compound **2a** was obtained with 95% purity (revealed by TLC), it was directly used for the next step.

ESI–MS: m/z = 116 (Calculated value for $C_6H_{16}N_2 = 116.0$).

*4.1.2.2. Synthesis of [2-(dibutylamino)ethyl]ammonium trifluoroacetate, compound **2b**.* Compound **2b** was synthesized following a similar procedure as described for **2a** synthesis above (0.144 g, 91.1% yield, $R_f = 0.1$, active in ninhydrin charring).

ESI–MS: m/z = 173 (Calculated value for $C_{10}H_{25}N_2 = 173.0$).

*4.1.2.3. Synthesis of [2-(dioctylamino)ethyl]ammonium trifluoroacetate, compound **2c**.* Compound **2c** was synthesized following a similar procedure as described for **2a** synthesis (0.271 g, 73.8% yield, $R_f = 0.25$, active in ninhydrin charring).

ESI–MS: m/z = 285 (Calculated value for $C_{18}H_{41}N_2 = 285.0$).

*4.1.2.4. Synthesis of [2-(didodecylamino)ethyl]ammonium trifluoroacetate, compound **2d**.* Compound **2d** was synthesized following a similar procedure as described for **2a** synthesis (0.264 g, 91.0% yield, $R_f = 0.4$ active in ninhydrin charring).

ESI–MS: m/z = 398 (Calculated value for $C_{26}H_{57}N_2 = 397.7$).

*4.1.2.5. Synthesis of [2-(dihexadecylamino)ethyl]ammonium trifluoroacetate, compound **2e**.* Compound **2e** was synthesized following a similar procedure as described for **2a** synthesis (0.260 g, 92.1% yield, $R_f = 0.5$ active in ninhydrin charring).

ESI–MS: m/z = 510 (Calculated value for $C_{34}H_{73}N_2 = 509.9$).

*4.1.3. Synthesis of compound **3***

Dexamethasone (0.47 g, 1.19 mmol) was dissolved with ethanol (93.5 mL), then water (37 mL) was added, followed by addition of sodium periodate (0.305 g, 1.42 mmol) and 2 M sulfuric acid (2.4 mL) in a 250 mL round-bottom flask. The resulting solution was left stirred at room temperature for 12 h. Then excess ethanol was removed *in vacuo* and water (36 mL), brine (19 mL) were added to the reaction mixture. The pH of the solution was adjusted to 12 with 1 M aqueous sodium hydroxide to dissolve the product in solution. The mixture was washed with DCM (3 × 100 mL) and then pH of the solution was adjusted to 3 with 1 M sodium bisulfate solution and finally extracted using ethyl acetate (2 × 100 mL), 1:1 DCM:ethyl acetate (2 × 100 mL). These organic extracts were combined and dried with anhydrous sodium sulfate followed by concentration *in vacuo* to get white compound **3** [17] (0.4 g, 97.0% yield, $R_f = 0.6$ in 10%, methanol–chloroform v/v).

^{1}H NMR (300 MHz, $CDCl_3$): δ/ppm = 0.92–0.97 [d, J = 7.1 Hz, 3H, $C_{20}\boldsymbol{H}$], 1.11 [s, 3H, $C_{18}\boldsymbol{H}$], 1.20–1.30 [m, 2H, $C_{15}\boldsymbol{H}$], 1.33–1.54 [m, 2H, $C_7\boldsymbol{H}$], 1.56 [s, 3H, $C_{19}\boldsymbol{H}$], 1.63–1.93 [m, 2H, $C_{12}\boldsymbol{H}$], 2.0–2.22 [m, 1H, $C_{14}\boldsymbol{H}$], 2.26–2.50 [m, 2H, $C_6\boldsymbol{H}$], 2.50–2.76 [m, 1H, $C_8\boldsymbol{H}$], 2.92–3.07 [m, 1H, $C_{16}\boldsymbol{H}$], 3.3–3.38 [m, 1H, $C_{11}\boldsymbol{H}$], 6.08 [s, 1H, $C_4\boldsymbol{H}$], 6.21–6.33 [d, 10.1 Hz, 1H, $C_2\boldsymbol{H}$], 7.27–7.39 [d, J = 10 Hz, 1H, $C_1\boldsymbol{H}$],

ESI–MS: m/z 379, 401 [MNa^+] (Calculated value for $C_{21}H_{27}O_5F = 378.43$).

*4.1.4. Syntheses of compounds **4a**–**e***

Syntheses of compounds **4a**–**e** followed a general chemistry procedure as described previously [29].

*4.1.4.1. Synthesis of compound **4a**.* Compound **3** (0.2 g, 0.53 mmol) was dissolved in 10 mL of dry DCM in a 25 mL round-bottomed flask and stirred over an ice bath for 15 min. To this, a mixture of 1-Ethyl-3-(3-dimethylaminopropyl) carbodiimide (EDCI) (0.101 g, 0.53 mmol) and Hydroxybenzotriazole (HOBT) (0.080 g, 0.52 mmol) were added and stirring was continued for another 30 min. Then compound **2a** (0.067 g, 0.57 mmol) was dissolved in 2 mL of dry DCM and added to the reaction mixture. DIPEA was added drop-wise to the ice cold reaction mixture (under stirring condition) until it became slightly basic. The resulting solution was left stirred for 18 h. The reaction mixture was dissolved in 30 mL chloroform and washed sequentially with water (3 × 30 mL), 1 N HCl (2 × 30 mL), saturated $NaHCO_3$ solution (3 × 30 mL) and brine (3 × 30 mL). The organic layer was dried with anhydrous sodium sulfate, filtered and the solvent from the filtrate was removed by rotary evaporation. Then mixture was purified by column chromatography using >200 mesh silica gel and 3% methanol–chloroform (v/v) as eluent. This yielded compound **4a** as a yellow gummy product (0.09 g, 35.8% yield, $R_f = 0.40$ in 10% methanol–chloroform (v/v).

^{1}H NMR (300 MHz, $CDCl_3$): δ/ppm = 0.55–0.67 [m, 9H, $-N(-CH_2-C\boldsymbol{H}_3)_2$, $C_{20}\boldsymbol{H}$], 1.02 [s, 3H, $C_{18}\boldsymbol{H}$], 1.30 [s, 3H, $C_{19}\boldsymbol{H}$], 1.41–1.78 [m, 4H, $C_7\boldsymbol{H}$, $C_{15}\boldsymbol{H}$], 1.79–2.44 [m, 6H, $C_6\boldsymbol{H}$, $C_8\boldsymbol{H}$, $C_{12}\boldsymbol{H}$, $C_{14}\boldsymbol{H}$], 2.48–2.64 [m, 4H, $-N(-C\boldsymbol{H}_2-CH_3)_2$], 2.66–2.82 [m, 2H, $-OC-HN-CH_2-C\boldsymbol{H}_2$], 2.95–3.21[m, 2H, $C_{11}\boldsymbol{H}$, $C_{16}\boldsymbol{H}$], 3.28–3.5 [m, 2H, $-OC-HN-C\boldsymbol{H}_2-CH_2$], 5.97 [s, 1H, $C_4\boldsymbol{H}$], 6.01–6.18 [d, J = 11 Hz, 1H, $C_2\boldsymbol{H}$], 6.99–7.07 [d, J = 10 Hz, 1H, $C_1\boldsymbol{H}$].

ESI–MS: m/z 477 (Calculated value for $C_{27}H_{41}N_2O_4F = 476.6$).

*4.1.4.2. Synthesis of compound **4b**.* Compound **3** (0.2 g, 0.53 mmol) was dissolved in 8 mL of dry DCM and 2 mL dry DMF in a 25 mL round-bottom flask and stirred over an ice bath for 15 min. To this, a mixture of EDCI (0.108 g, 0.63 mmol) and HOBT (0.08 g, 0.52 mmol) was added and stirring was continued for another 30 min. Then, compound **2b** (0.067 g, 0.57 mmol) was dissolved in 2 mL of dry DCM and added to the reaction mixture. DIPEA was added drop-wise to the ice cold reaction mixture (under stirring condition) until it became slightly basic. The resulting mixture was stirred for 20 h. Then work up was done following a similar procedure as used for compound **4a**. The mixture was purified by column chromatography using 60–120 mesh silica gel and 2.2% methanol–chloroform (v/v) as eluent. This yielded compound **4b** as a yellowish product (0.2 g, 70.0% yield, R_f = 0.5 in 10% methanol–chloroform (v/v).

^{1}H NMR (300 MHz, $CDCl_3$): δ/ppm = 0.81–1.00 [m, 9H, $-N(-CH_2-(CH_2)_2-CH_3)_2$, $C_{20}H$], 1.05 [s, 3H, $C_{18}H$], 1.26-1.46 [m, 9H, $-N(-CH_2-CH_2-CH_2-CH_3)_2$, C_7H, $C_{19}H$], 1.47–1.92 [m, 7H,$-N(-CH_2-CH_2-CH_2-CH_3)_2$, $C_{14}H$, $C_{15}H$], 2.05–2.74 [m, 6H, C_6H, C_8H, $C_{12}H$, $C_{16}H$], 2.78–2.90 [t, J = 7.0 Hz, 4H, $-N(-CH_2-CH_2-CH_2-CH_3)_2$], 2.94–3.19 [m, 2H, $-OC-HN-CH_2-CH_2$], 3.22–3.42 [m, 2H, $-OC-HN-CH_2-CH_2$], 3.82–4.06 [m, 1H, $C_{11}H$], 6.04 [s, 1H, C_4H], 6.24–6.30 [d, J = 10 Hz, 1H, C_2H], 7.27 [s, 1H, C_1H].

ESI–MS: m/z 533 (Calculated value for $C_{31}H_{49}N_2O_4F$ = 532.7).

*4.1.4.3. Synthesis of compound **4c**.* Compound **3** (0.3 g, 0.8 mmol) was dissolved in 12 mL dry dimethyl formamide (DMF) and 5 mL dimethyl sulfoxide (DMSO) in a 25 mL round-bottom flask and the turbid like mixture was stirred over an ice bath for 15 min. To this, a mixture of EDCI (0.271 g, 0.95 mmol) and HOBT (0.151 g, 0.78 mmol) was added, and stirring was continued for another 30 min. Then, compound **2c** (0.113 g, 0.390 mmol) was dissolved in 2 mL of dry DCM and added to the reaction mixture. DIPEA was added drop-wise to the ice cold reaction mixture (under stirring condition) until it became slightly basic. The resulting mixture was stirred for overnight at room temperature. The work up was done following a similar procedure as used for compound **4a**. The mixture was purified by column chromatography using 60–120 mesh silica gel and 2.0% methanol–chloroform (v/v) as eluent. This yielded compound **4c** as a whitish product (0.2 g, 39.1% yield, R_f = 0.55 in 10% methanol–chloroform (v/v).

^{1}H NMR (300 MHz, $CDCl_3$): δ/ppm = 0.68–0.93 [m, 9H, $-N(-CH_2-CH_2-(CH_2)_4-CH_2-CH_3)_2$, $C_{20}H$], 1.02 [s, 3H, $C_{18}H$], 1.08–1.31 [m, 21H, $-N(-CH_2-CH_2-(CH_2)_4-CH_2-CH_3)_2$, C_7H, $C_{19}H$], 1.33–1.86 [m, 11H, $-N(-CH_2-CH_2-(CH_2)_4-CH_2-CH_3)_2$, $C_{14}H$, $C_{15}H$], 1.91–2.76 [m, 10H, $-N(-CH_2-CH_2-(CH_2)_4-CH_2-CH_3)_2$, C_6H, C_8H, $C_{12}H$, $C_{16}H$], 2.91–3.04 [t, J = 6.9 Hz, 2H, $-OC-HN-CH_2-CH_2$], 3.10–3.30 [m, 2H, $-OC-HN-CH_2-CH_2$], 3.34–3.59 [m, 1H, $C_{11}H$], 5.99 [s, 1H, C_4H], 6.15–6.23 [d, J = 10.1 Hz, 1H, C_2H], 7.18–7.26 [d, J = 10.1 Hz, 1H, C_1H].

ESI–MS: m/z 645 (Calculated value for $C_{39}H_{65}N_2O_4F$ = 644.9).

*4.1.4.4. Synthesis of compound **4d**.* Compound **3** (0.250 g, 0.66 mmol) was dissolved in 10 mL of dry DCM in a 25 mL round-bottom flask and mixture was stirred over an ice bath for 15 min. To this, a mixture of EDCI (0.126 g, 0.65 mmol) and HOBT (0.099 g, 0.65 mmol) was added, and stirring was continued for another 30 min. Then compound **2d** (0.211 g, 0.53 mmol) was dissolved in 2 mL of dry DCM and added to the reaction mixture. DIPEA was added drop-wise to the ice-cold reaction mixture (under stirring condition) until it became slightly basic. The resulting mixture was stirred for 24 h. Then work up was done following a similar procedure as used for compound **4a**. The reaction mixture was evaporated and purified by column chromatography using 60–120 mesh silica gel and 1% methanol–chloroform (v/v) as eluent. This yielded compound **4d** as a yellow gummy product (0.3 g, 58.8% yield, R_f = 0.6 in 10% methanol–chloroform (v/v).

^{1}H NMR (300 MHz, $CDCl_3$): δ/ppm = 0.75–0.90 [m, 9H, $-N(-CH_2-CH_2-(CH_2)_9-CH_3)_2$, $C_{20}H$], 1.02 [s, 3H, $C_{18}H$], 1.11–1.29 [m, 41H, $-N(-CH_2-CH_2-(CH_2)_9-CH_3)_2$, C_7H, $C_{19}H$], 1.37–1.98 [m, 10H, $-N(-CH_2-CH_2-(CH_2)_9-CH_3)_2$, C_8H, $C_{12}H$, $C_{14}H$, $C_{15}H$], 2.07–2.91 [m, 9H, $N(-CH_2-CH_2-(CH_2)_9-CH_3)_2$, $-OC-HN-CH_2-CH_2$, C_6H, $C_{16}H$], 3.20–3.33 [t, J = 6.6 Hz, 2H, $-OC-HN-CH_2-CH_2$], 3.38–3.56 [m, 1H, $C_{11}H$], 6.00 [s, 1H, C_4H], 6.16–6.26 [d, J = 7.9 Hz, 1H, C_2H], 7.12–7.33 [d, J = 7.9 Hz, 1H, C_1H].

ESI–MS: m/z 757 (Calculated value for $C_{47}H_{81}N_2O_4F$ = 757.1).

*4.1.4.5. Synthesis of compound **4e**.* Compound **3** (0.2 g, 0.53 mmol) was dissolved in 10 mL of dry DCM in a 25 mL round-bottomed flask and mixture was stirred over an ice bath for 15 min. To this, a mixture of EDCI (0.101 g, 0.52 mmol) and HOBT (0.079 g, 0.52 mmol) was added and stirring was continued for another 30 min. Then compound **2e** (0.215 g, 0.42 mmol) was dissolved in 2 mL of dry DCM and added to the reaction mixture. DIPEA was added drop-wise to the ice cold reaction mixture (under stirring condition) until it became slightly basic. The resulting mixture was stirred for 48 h. Then work up was done following a similar procedure as used for compound **4a**. The reaction mixture was evaporated and purified by column chromatography using 60–120 mesh silica gel and 0.9% methanol–chloroform (v/v) as eluent. This yielded compound **4e** as a gummy product (0.19 g, 41.3% yield, R_f = 0.65 in 10% methanol–chloroform (v/v).

^{1}H NMR (300 MHz, $CDCl_3$): δ/ppm = 0.75–0.94 [m, 9H, $-N(-CH_2-CH_2-(CH_2)_{13}-CH_3)_2$, $C_{20}H$], 0.99 [s, 3H, $C_{18}H$], 1.04–1.30 [m, 57H, $-N(-CH_2-CH_2-(CH_2)_{13}-CH_3)_2$, C_7H, $C_{19}H$], 1.34–1.83 [m, 10H, $-N(-CH_2-CH_2-(CH_2)_{13}-CH_3)_2$, C_8H, $C_{12}H$, $C_{14}H$, $C_{15}H$,], 1.91–2.89 [m, 9H, $-N(-CH_2-CH_2-(CH_2)_{13}-CH_3)_2$, $-OC-HN-CH_2-CH_2$,C_6H, $C_{16}H$], 2.9–3.10 [t, J = 6.4 Hz, 2H, $-OC-HN-CH_2-CH_2$], 3.15–3.44 [m, 1H, $C_{11}H$], 5.99 [s, 1H, C_4H], 6.11–6.29 [d, J = 9.9 Hz, 1H, C_2H], 7.15–7.37[d, J = 9.9 Hz, 1H, C_1H].

ESI–MS: m/z 870 (Calculated value for $C_{56}H_{97}N_2O_4F$ = 869.3).

*4.1.5. Syntheses of compounds **5a–e***

Syntheses of compounds **5a–e** followed a general protocol as exemplified below.

*4.1.5.1. Synthesis of compound **5a**.* Compound **4a** (0.1 g, 0.21 mmol) was dissolved in 8 mL methyl iodide (MeI), then potassium carbonate (K_2CO_3) (0.115 g, 0.82 mmol) was added to the mixture in a 15 mL round-bottomed flask. The reaction mixture was stirred for 12 h at room temperature. Then it was filtered, concentrated and the residue was purified by column chromatography (using 60–120 mesh silica gel and 6–7% methanol–chloroform (v/v) as eluent), followed by chloride ion exchange chromatography (using Amberlite IRA-400Cl resin and methanol as eluent). This yielded compound **5a** as a colorless gummy solid (0.32 g, 31.0% yield, R_f = 0.2 in 10% methanol–chloroform, v/v).

^{1}H NMR (300 MHz, $CDCl_3$): δ/ppm = 0.90–0.95 [d, J = 7.1 Hz, 3H, $C_{20}H$], 1.04 [s, 3H, $C_{18}H$], 1.17–1.29 [m, 2H, C_7H], 1.34–1.44 [t, J = 6.6 Hz, 6H, $-N(-CH_2-CH_3)_2$], 1.48–1.90 [m, 6H, $C_{14}H$, $C_{15}H$, $C_{19}H$], 2.06–2.73 [m, 6H, C_6H, C_8H, $C_{12}H$, $C_{16}H$], 3.04 [s, 3H, $-OC-HN-CH_2-CH_2-N-CH_3$], 3.33–3.48 [m, 4H, $-N(-CH_2-CH_3)_2$], 3.56–3.71 [m, 5H, $-OC-HN-CH_2-CH_2$, $C_{11}H$], 6.09 [s, 1H, C_4H], 6.25–6.33 [d, J = 9.8 Hz, 1H, C_2H], 7.34–7.42 [d, J = 9.8 Hz, 1H, C_1H].

^{13}C NMR (75 MHz, $CDCl_3$): δ/ppm = [187.0 (C_3), 174.6 (C_{21}), 167.3(C_5), 154.2(C_1), 129.3(C_2), 124.7(C_4), 103.8(C_9, doublet), 87.7(C_{17}), 71.0 (C_{11}), 59.4 {$-N-CH_2-CH_3$}$_2$, 57.1 ($O=C-NH-CH_2-CH_2-$), 56.8 {$-(+)N-CH_3$}, 48.2 (C_{10}), 44.1 (C_{14}), 36.2

(C_{16}), 35.2 (O=C–NH–**C**H_2–CH_2–), 34.3 (C_{12}), 33.1(C_{13}), 31.9 (C_8), 31.1(C_{15}), 29.6 (C_6), 27.9 (C_7), 22.6 (C_{19}), 15.8(C_{18}), 14.1(C_{20}), 8.0(–N–CH_2–**C**H_3)].

ESI–MS: *m/z* 491.

ESI–HRMS = 491.3298 (calculated mass for $C_{28}H_{44}N_2O_4F$ = 491.3285).

HPLC purity = 99.53%.

*4.1.5.2. Synthesis of compound **5b**.* Compound **5b** was synthesized following a similar procedure as described for **5a** synthesis above (26.5% yield, R_f = 0.48 in 10% methanol–chloroform, v/v).

^{1}H NMR (300 MHz, $CDCl_3$): δ/ppm = 0.87–0.92 [d, J = 7.7 Hz, 3H, C_{20}***H***], 1.01–1.08 [t, J = 7.2 Hz, 9H,–N(–CH_2–CH_2–CH_2–**C**H_3)$_2$, C_{18}***H***], 1.17–1.51 [m, 6H, –N(–CH_2–CH_2–C***H***$_2$–CH_3)$_2$, C_7***H***], 1.55–1.91 [m, 9H, C_8***H***, C_{12}***H***, C_{14}***H***, C_{15}***H***, C_{19}***H***], 2.12–2.74 [m, 7H, –N(–CH_2–C***H***$_2$–CH_2–CH_3)$_2$, C_6***H***, C_{16}***H***], 3.06 [s, 3H, –OC–HN–CH_2–CH_2–N–C***H***$_3$], 3.24–3.44 [m, 7H,–N(–C***H***$_2$–CH_2–CH_2–CH_3)$_2$,–OC–HN–CH_2–C***H***$_2$, C_{11}***H***], 3.56–3.62 [d, J = 6.7 Hz, 2H,–OC–HN–C***H***$_2$–CH_2], 6.08 [s, 1H, C_4***H***], 6.25–6.33 [d, J = 11 Hz, 1H, C_2***H***], 7.38–7.43 [d, J = 11.5 Hz, 1H, C_1***H***].

^{13}C NMR (75 MHz, $CDCl_3$): δ/ppm = [186.7 (C_3), 173.9 (C_{21}), 167.0 (C_5), 153.8 (C_1), 129.1 (C_2), 124.6 (C_4), 101.2 (C_9, doublet), 87.9 (C_{17}), 70.1 (C_{11}), 62.1{–N–**C**H_2–$(CH_2)_2$–CH_3}$_2$, 61.8 (O=C–NH–CH_2–**C**H_2–), 60.5{–(+)N–**C**H_3}, 48.0 (C_{10}), 44.0 (C_{14}), 36.1(C_{16}), 35.2 (O=C–NH–**C**H_2–CH_2–), 34.0 (C_{13}), 32.8 (C_8), 32.3 (C_{15}), 30.9 (C_6), 29.5 (C_7), 24.1{–N–CH_2–**C**H_2–CH_2–CH_3}$_2$, 19.5 (C_{19}), 17.6 {–N–CH_2–CH_2–**C**H_2–CH_3}$_2$, 16.0 (C_{18}), 14.0(C_{20}), 13.8 {–N–$(CH_2)_3$–**C**H_3}].

ESI–MS: *m/z* 547.

ESI–HRMS = 547.3936 (calculated mass for $C_{32}H_{52}N_2O_4F$ = 547.3911).

HPLC purity = 97.46%.

*4.1.5.3. Synthesis of compound **5c**.* Compound **5c** was synthesized following a similar procedure as described for compound **5a** (20.5% yield, R_f = 0.55 in 10% methanol–chloroform, v/v).

^{1}H NMR (300 MHz, $CDCl_3$): δ/ppm = 0.81–0.97 [m, 9H, J = 6.7 Hz, –N(–CH_2–CH_2–$(CH_2)_5$–C***H***$_3$)$_2$, C_{20}***H***], 1.02 [s, 3H, C_{18}***H***], 1.16–1.42 [m, 25H, –N(–CH_2–CH_2–(C***H***$_2$)$_5$–CH_3)$_2$, C_7***H***, C_{19}***H***], 1.45–1.90 [m, 10H,–N(–CH_2–C***H***$_2$–$(CH_2)_5$–CH_3)$_2$, C_8***H***, C_{12}***H***, C_{14}***H***, C_{15}***H***,], 2.05–2.75 [m, 7H, –N(–C***H***$_2$–CH_2–$(CH_2)_5$–CH_3)$_2$, C_6***H***, C_{16}***H***], 3.06 [s, 3H, –OC–HN–CH_2–CH_2–N–C***H***$_3$], 3.19–3.30 [t, 2H, J = 6.7 Hz, –OC–HN–CH_2–C***H***$_2$], 3.35–3.59 [m, 3H,–OC–HN–C***H***$_2$–CH_2, C_{11}***H***], 6.07 [s, 1H, C_4***H***], 6.27–6.33 [d, J = 10.1 Hz, 1H, C_2***H***], 7.35–7.40 [d, J = 10.1 Hz, 1H, C_1***H***].

^{13}C NMR (125 MHz, $CDCl_3$): δ/ppm = [186.9 (C_3), 174.3(C_{21}), 167.1(C_5), 154.2 (C_1), 129.3 (C_2), 124.7 (C_4), 103.8 (C_9, doublet), 87.8 (C_{17}), 70.6 (C_{11}), 62.3 {–N–**C**H_2–$(CH_2)_6$–CH_3}$_2$, 61.7 (O=C–NH–CH_2–**C**H_2–), 61.4 {–(+)N–**C**H_3}, 48.2 (C_{10}), 44.2 (C_{14}), 36.7 (C_{16}), 35.1 (O=C–NH–**C**H_2–CH_2–), 35.2 (C_{13}), 34.4 (C_8), 33.0 (C_{15}), 32.7{–N–$(CH_2)_5$–**C**H_2–CH_2 –CH_3}$_2$, 31.5 (C_6), 31.2{–N–$(CH_2)_3$–**C**H_2–$(CH_2)_3$–CH_3}$_2$, 29.6 (C_7), 27.9 {–N–$(CH_2)_4$–**C**H_2–$(CH_2)_2$–CH_3}$_2$, 26.3 {–N–$(CH_2)_2$–**C**H_2–$(CH_2)_4$–CH_3}$_2$, 23.0 (C_{19}), 22.5 {–N–$(CH_2)_6$–**C**H_2–CH_3}$_2$, 22.3{–N–CH_2–**C**H_2–$(CH_2)_5$–CH_3}$_2$, 17.0 (C_{18}), 16.0 (C_{20}), 14.0{–N–$(CH_2)_7$–**C**H_3}].

ESI–MS: *m/z* 659.

ESI–HRMS = 659.5155 (calculated mass for $C_{40}H_{68}N_2O_4F$ = 659.5157).

HPLC purity = 98.41%.

*4.1.5.4. Synthesis of compound **5d**.* Compound **5d** was synthesized following a similar procedure as described for compound **5a** (66.6% yield, R_f = 0.68 in 10% methanol–chloroform, v/v).

^{1}H NMR (300 MHz, $CDCl_3$): δ/ppm = 0.87–0.93 [t, 9H, J = 6.9, –N(–CH_2–CH_2–$(CH_2)_9$–C***H***$_3$)$_2$, C_{20}***H***], 1.02 [s, 3H, C_{18}***H***], 1.21–1.39 [m, 41H, –N(–CH_2–CH_2–(C***H***$_2$)$_9$–CH_3)$_2$, C_7***H***, C_{19}***H***], 1.57–1.90 [m, 10H, –N(–C***H***$_2$–CH_2–$(CH_2)_9$–CH_3)$_2$, C_8***H***, C_{12}***H***, C_{14}***H***, C_{15}***H***], 1.97–2.50 [m, 7H, –N(–C***H***$_2$–CH_2–$(CH_2)_9$–CH_3)$_2$, C_6***H***, C_{16}***H***], 3.05 [s, 3H, –OC–HN–CH_2–CH_2–N–C***H***$_3$], 3.11–3.28 [t, 2H, J = 6.7 Hz, –OC–HN–CH_2–C***H***$_2$], 3.44–3.74 [m, 3H,–OC–HN–C***H***$_2$–CH_2, C_{11}***H***], 6.04 [s, 1H, C_4***H***], 6.27–6.32 [d, J = 10.3 Hz, 1H, C_2***H***], [s, 1H, C_1***H***].

^{13}C NMR (125 MHz, $CDCl_3$): δ/ppm = [186.7 (C_3), 174.1(C_{21}), 167.0 (C_5), 153.9 (C_1), 129.2 (C_2), 124.6 (C_4), 103.8 (C_9, doublet), 87.5 (C_{17}), 71.1(C_{11}), 62.0 {–N–**C**H_2–$(CH_2)_{10}$–CH_3}$_2$, 61.6 (O=C–NH–CH_2–**C**H_2–), 60.9{–(+)N–**C**H_3}, 48.7 (C_{10}), 44.0 (C_{14}), 36.0 (C_{16}), 35.1 (O=C–NH–CH_2–CH_2–), 34.4 (C_{13}), 34.1(C_8), 32.8 (C_{15}), 32.5{–N–$(CH_2)_9$–**C**H_2–CH_2–CH_3}$_2$, 31.7 (C_6), 31.0{–N–$(CH_2)_7$–**C**H_2–$(CH_2)_3$–CH_3}$_2$, 29.3 {–N–$(CH_2)_6$–**C**H_2–$(CH_2)_4$–CH_3}$_2$, 29.29{–N–$(CH_2)_5$–**C**H_2–$(CH_2)_5$–CH_3}$_2$, 29.2 {–N–$(CH_2)_3$–**C**H_2–$(CH_2)_7$–CH_3}$_2$, 29.0 (C_7), 27.7{–N–$(CH_2)_4$–**C**H_2–$(CH_2)_6$–CH_3}$_2$, 26.2{–N–$(CH_2)_2$–**C**H_2–$(CH_2)_8$–CH_3}$_2$, 23.0 (C_{19}), 22.5{–N–$(CH_2)_{10}$–**C**H_2–CH_3}$_2$, 22.1{–N–CH_2–**C**H_2–$(CH_2)_9$–CH_3}$_2$, 16.9 (C_{18}), 15.6 (C_{20}), 13.9{–N–$(CH_2)_{11}$–**C**H_3}].

ESI–MS: *m/z* 771.

ESI–HRMS = 771.6446 (calculated mass for $C_{48}H_{84}N_2O_4F$ = 771.6415).

HPLC purity = 95.85%.

*4.1.5.5. Synthesis of **5e**.* Compound **5e** was synthesized following the similar procedure as described for compound **5a** (36.8% yield, R_f = 0.8 in 10% methanol–chloroform, v/v).

^{1}H NMR (300 MHz, $CDCl_3$): δ/ppm = 0.70–0.87 [m, 9H, J = 6.9 Hz, –N(–CH_2–CH_2–$(CH_2)_{13}$–C***H***$_3$)$_2$, C_{20}***H***], 0.98 [s, 3H, C_{18}***H***], 1.07–1.36 [m, 57H, –N(–CH_2–CH_2–(C***H***$_2$)$_{13}$–CH_3)$_2$, C_7***H***, C_{19}***H***], 1.41–1.81 [m, 10H, –N(–C***H***$_2$–CH_2–$(CH_2)_{13}$–CH_3)$_2$, C_8***H***, C_{12}***H***, C_{14}***H***, C_{15}***H***], 1.84–2.80 [m, 7H, –N(–C***H***$_2$–CH_2–$(CH_2)_9$–CH_3)$_2$, C_6***H***, C_{16}***H***], 3.01 [s, 3H, –OC–HN–CH_2–CH_2–N–C***H***$_3$], 3.11–3.24 [t, 2H, J = 6.7 Hz, –OC–HN–CH_2–C***H***$_2$], 3.29–3.56 [m, 3H,–OC–HN–C***H***$_2$–CH_2, C_{11}***H***], 6.02 [s, 1H, C_4***H***], 6.20–6.28 [d, J = 9.4 Hz, 1H, C_2***H***], 7.30–7.38 [d, J = 9.9 Hz, 1H, C_1***H***], ^{13}C NMR (125 MHz, $CDCl_3$): δ/ppm = [186.9 (C_3), 174.4 (C_{21}), 167.0 (C_5), 153.9 (C_1), 129.3 (C_2), 124.7 (C_4), 103.6 (C_9, doublet), 87.5 (C_{17}), 71.4 (C_{11}), 62.0 {–N–**C**H_2–$(CH_2)_{14}$–CH_3}$_2$, 61.7 (O=C–NH–CH_2–**C**H_2–), 61.1 {–N(+)–**C**H_3}, 48.4 (C_{10}),44 (C_{14}), 37.3 (C_{16}), 37.0 (O=C–NH–**C**H_2–CH_2–), 35.9(C_{13}), 35.2 (C_8), 32.6(C_{15}), 32.9 {–N–$(CH_2)_{13}$-**C**H_2–CH_2–CH_3}$_2$, 31.9 (C_6), 31.3 {-N-$(CH_2)_{11}$-**C**H_2-$(CH_2)_3$–CH_3}$_2$, 31.1 {-N-$(CH_2)_{10}$-**C**H_2-$(CH_2)_4$–CH_3}$_2$, 30.1 {-N-$(CH_2)_9$-**C**H_2-$(CH_2)_5$–CH_3}$_2$, 30.0 {-N-$(CH_2)_8$-**C**H_2-$(CH_2)_6$–CH_3}$_2$, 29.6 {-N-$(CH_2)_7$-**C**H_2-$(CH_2)_7$–CH_3}$_2$, 29.4 {-N-$(CH_2)_6$-**C**H_2-$(CH_2)_8$–CH_3}$_2$, 24.3 {-N-$(CH_2)_5$-**C**H_2-$(CH_2)_9$–CH_3}$_2$, 29.0 {-N-$(CH_2)_3$-**C**H_2-$(CH_2)_{11}$–CH_3}$_2$, 26.3(C_7), 22.9 {-N-$(CH_2)_4$-**C**H_2-$(CH_2)_{10}$–CH_3}$_2$, 22.6 {-N-$(CH_2)_2$-**C**H_2-$(CH_2)_{12}$–CH_3}$_2$, 22.2 (C_{19}), 19.6 {-N-CH_2-$(CH_2)_{13}$–**C**H_2–CH_3}$_2$, 17.0 {-N-CH_2-**C**H_2-$(CH_2)_{13}$–CH_3}$_2$, 15.4 (C_{18}), 14.4 (C_{20}), 14.1{-N-$(CH_2)_{15}$-**C**H_3}].

ESI–MS: *m/z* 884.

ESI–HRMS = 883.7663 (calculated mass for $C_{56}H_{100}N_2O_4F$ = 883.7667).

HPLC purity = 97.41%.

4.2. Biological experiments

4.2.1. Antibodies

Caspase 3 (ab44976), Smac/Diablo (ab 32023), Mdm2 (ab 38618), XIAP were purchased from Abcam, UK; BAX (PA5-17806), Bcl-2 (MA5-14937), Akt-1 (MA5-14898), p-Akt (ser 473,PA1-14032), Caspase 9 (PA5-16358), Active Caspase 3 (PA1-29157), STAT3 (PA5-16187), p-STAT3 (Tyr705, MA5-1118), p-STAT3 (Ser727, PA1-14393), JAK2 (OPA1-03052A), JAK3, Cytochrome C (PA1-9586), Caspase 7, β-Actin (PA5-16914) and goat anti rabbit IgG alkaline

Phosphatase-conjugated (31340) were purchased from Pierce Protein Research, USA; p53 (#2524), GAPDH (#5174),were purchased from Cell Signaling Technology; Anti-KDR/Flk-1/VEGFR2 (07-158) was purchased from Millipore; VE-cadherin (sc-9989), and mouse mouse-anti-rabbit IgG-FITC (sc-2359), goat anti-rabbit IgG-FITC (sc-3839), Anti-GR (sc-8992), were purchased from Santa Cruz Biotechnology; Goat anti-mouse IgG Alkaline Phosphatase (DC05L) were purchased from Calbiochem, Germany, IL-6 assay kit was purchased from e-Bioscience, USA.

4.2.2. Samples preparation and treatment

These Synthesized compounds were dissolved in cell culture grade DMSO to get a primary stock. Then stocks were progressively diluted with DMSO to make secondary stock and finally working concentrations of those compounds were obtained by adding the secondary DMSO stocks in 10% fetal bovine serum (FBS) containing cell culture medium. The concentration of DMSO in 10% FBS containing working medium never exceeded more than 1%. For the cell viability studies an amount of 100 μL of cell culture solutions containing respective concentrations of derivatives were added to each well of 96-well plates and few wells were kept untreated. For quantification of apoptosis studies an amount of 1.5 mL of culture medium containing respective concentrations of compounds were added to each well of 6-well plates.

4.2.3. Cell culture

MCF-7 (human breast adenocarcinoma), B16F10 (murine melanoma), CHO (Chinese hamster ovary), human lung carcinoma (A549), Human embryo kidney (HEK293T) cell lines were purchased from the American Type Cell Culture (ATCC, USA) and National Center for Cell Sciences (Pune, India). Freshly isolated mouse skin fibroblast (FB) cell was obtained from Center for Cellular and Molecular Biology (Hyderabad, India) and was grown in mycoplasma free condition. Cells were cultured in DMEM supplemented with 10% US origin FBS (Lonza, USA), 50 μg/mL penicillin, 50 μg/mL streptomycin and 100 μg/mL kanamycin at 37 °C in a humidified condition of 5% CO_2 in air. Cultured healthy cells of 75–85% confluency were used for experiments. Cells were trypsinized, counted and seeded, in 6-well plates for quantification of apoptosis studies, 96-well plates for cell viability studies and in 25 cm^2 or 75 cm^2 tissue culture flasks for Western blot studies. The cells were kept to adhere overnight before they were used for experiments.

4.2.4. Cytotoxicity studies

Cytotoxicity assay of the compounds were determined by the reduction of 3-(4,5-dimethylthiazol-2-yl)-2,5-diphenyltetrazolium bromide (MTT). Briefly, cells were plated well in 96-well plates with density of 5000 cells/well usually 12–18 h before experiments. Solutions containing respective concentrations of following compounds were added in at least triplicate wells or more. In the screening experiments dexamethasone derivatives (DXn) were continuously treated to the cells for 72 h. Following termination of treatment, cells were washed with Phosphate buffer saline (PBS) and assayed for viability using MTT. Results were represented as percentage of viability = {[A550 (treated cells) − background]/[A550 (untreated cells) − background]} × 100.

4.2.5. Glucocorticoid receptor (GR) down-regulation by siRNA delivery

GR down-regulation siRNA was based on following a similar procedure as described earlier [14]. Briefly, B16F10 and A549 cells were plated with a density of 2.5×10^5 cells per well in a 6-well plate usually between 12 and 18 h before transfection. Then 25 pmol of negative control siRNA (Qiagen) (diluted to 50 μL with serum free DMEM) or 25 pmol of GR-siRNA (Santa Cruz Biotechnology) (diluted to 50 μL with serum free DMEM) were complexed with 2.5 μL of Lipofectamine 2000 (Invitrogen) for 15–20 min. An amount of 900 μL siRNA-complex containing serum free DMEM was added to the six well plates and kept for 4 h. Then, 10% FBS containing DMEM was freshly added into the same well and left the plates as such for 36 h. After that cells were washed with PBS and harvested, counted, and again seeded at a density of 5000 cells/well in 96-well plates for MTT assay. However, after 12 h cells in 96-well plate cells were either kept untreated or treated with 10 μM DX8 for another 36 h in B16F10 and A549 experiment. For this study viability assay was performed after 36 h of compound treatment. After completion of treatment the cells were washed assayed for viability using MTT as described earlier.

GR siRNA(m) [cat no. sc-35506]	
1060	CCACUAUGACAUGAAUAC
1971	GCAUGUAUGACCAAUGUA
2103	GCCAAGAGUUAUUUGAUG
GR siRNA(H) [cat no.sc-35505]	
2096	GGCUUCAGGUAUCUUAUG
2178	CCAAGAGCUAUUUGAUGA
3202	CUCCAGUAUUCUUGUCAA
Control siRNA [Qiagen Inc.]	
UUCUCCGAACGUGUCACGUTT	
ACGUGACACGUUCGGAGAATT	

4.2.6. Flow cytometric analysis

The remaining cells after seeding from the above experiment were used to evaluate the extent of down-regulation of GR by flow cytometry. They were re-plated, and after 48 h they were harvested, washed, fixed with 2% formaldehyde in PBS for 10–15 min, and then permeabilized with 0.01% triton-x in PBS for 5–10 min at room temperature [14]. Then they were collected by centrifugation, washed, and treated with rabbit raised full-length glucocorticoid receptor primary antibody obtained from Santa Cruz Biotechnology for A549 cells and from Cell Signaling Technology for B16F10 (at 1:100 dilutions, in PBS containing 2% fetal bovine serum) at 4 °C for 2 h. After incubation, cells were collected by centrifugation, washed, and treated with FITC-conjugated goat-anti rabbit secondary antibody (Santa Cruz Biotechnology) at 1:500 dilution (in PBS containing 2% fetal bovine serum) and incubated at 4 °C for 1 h in the dark. Finally cells were washed and analyzed using a flow cytometer (FACS Canto II, Becton Dickinson, San Jose, CA, U.S.) and data were analyzed with FCS Express V3 software. Minimum of 10,000 events were gated per sample.

For p53 level detection in B16F10 cells, cells were treated with 10 μM DX8 and Dex for 48 h. Following which cells were harvested, washed, fixed with 2% formaldehyde in PBS for 10–15 min, and then permeabilized with 0.01% triton-x in PBS for 5–10 min at room temperature. As described above, cells were collected and treated with mouse monoclonal p53 antibody (Cell Signaling Technology, USA) at 1: 100 dilution (in PBS containing 2% fetal bovine serum) and incubated at 4 °C for 2 h in the dark. The cells were washed with PBS and incubated with PE-conjugated goat-anti-mouse secondary antibody for 1 h at 4 °C. Cells were finally washed and analyzed using a flow cytometer (FACS Canto II, Becton Dickinson, San Jose, CA, U.S.) and data were analyzed with FCS Express V3 software. Minimum of 10,000 events were gated per sample.

4.2.7. Quantification of apoptosis studies

The annexin V-FITC-labeled apoptosis detection kit (Sigma) was used to detect and quantify apoptosis by flow cytometry as per manufacturer's instructions. In brief, cells (2×10^5 cells/well) were seeded in six-well plates and cultured overnight in 10% serum

containing complete medium. After 16–18 h cells were kept untreated (UT) or treated with 10 μM Dex or 10 μM DX8 for 48 h. Then the cells were harvested and collected by centrifugation for 5 min at 1000 g. Cells were then re-suspended at a density of 1×10^6 cells/mL in 1× binding buffer and stained simultaneously with FITC-labeled annexin V (25 ng/mL) and propidium iodide (50 ng/mL). Cells were analyzed using a flow cytometer (FACS Canto II), and data were analyzed with FCS Express V3 software. Minimum of 10,000 events were gated per sample.

4.2.8. Preclinical studies using C57BL6/J mice

Female C57BL6/J mice were obtained from National Institute of Nutrition (NIN, Hyderabad, India). The protocols for animal experimentation were approved through Institutional Animal Ethical Committee. Female C57BL6/J mice, 8–10 weeks old, were subcutaneously inoculated with 2.2×10^5 B16F10 cells in the lower right abdomen. Fourteen days following cancer cell implantation, mice were grouped as per treatment. The groups were as follows: (i) group kept untreated, UT (four mice) (ii) group treated with Dex (four mice) and (iii) group treated with DX8 (four mice). For DX8 treatment group an amount of 20 mg/kg compound in 5% glucose having DMSO concentration 5% was injected and for Dex treatment group equivalent amount of DX8 equal to an amount of 12 mg/kg in 5% glucose having DMSO concentration 5% was injected. Five intraperitoneal injections with every alternate day were administered. Tumors were measured every alternate day and tumor sizes were expressed in volume (mm^3) and calculated using the formula ($0.5\ ab^2$), where 'a' is the longest dimension and 'b' is the shortest dimension of the tumors. Animals were humanely euthanized when the average tumor volume of the untreated (UT) group reached~2000 mm^3.

4.2.9. TUNEL assay

After completion of the above experiment one mouse from each group was sacrificed for detection of apoptosis in tumor tissues. The tumors were frozen in Jung tissue freeze medium (Leica Microsystem Germany) followed by cryo-sectioning of 10 μm thin sections using Leica CM1850 Cryostat (Germany). The sections were fixed with 4% formalin for 15 min and TUNEL assayed using Dead-End fluorometric TUNEL assay kit (Promega, Madison, WI) as per manufacturer's protocol. The same cryosections used for TUNEL assay were again considered for blood vessel staining by VE-cadherin. The tissue sections were washed and incubated for 2 h at 4 °C with VE-cadherin mouse monoclonal antibody (Santa Cruz) followed by one hour incubation with Texas Red conjugated goat-anti-mouse secondary antibody. Images were acquired in Nikon TE 2000E microscope at 10× magnification. Duplicate panel in TUNEL assay of DX8 treated tumor section is to represent signature of apoptosis in both tumor and tumor associated endothelial cells in two different areas of tumor section.

4.2.10. VEGFR2-downregulation analysis

VEGFR2 down-regulation was based on a similar procedure as described earlier [30]. Thin 10 μm tumor sections were fixed and incubated with VEGFR2-rabbit monoclonal antibody for 2 h at 4 °C. This was followed by washing with PBS (3 × 10 min) and then kept in goat anti-rabbit FITC conjugated secondary antibody for another 45 min. The sections were visualized using Nikon TE 2000E microscope at 10× magnification.

4.2.11. Western blot

For this study, B16F10 cells were treated with Dex, DX8 (10 μM) or kept untreated for continuously 48 h in 10% FBS containing DMEM. Following treatment whole cell lysates from both the cells were prepared as follows: Cells were lysed 50 mM Tris–HCl, pH 7.4, 0.15 M NaCl, 1% Nonidet P-40, 0.5% sodium deoxycholate, and 0.1% SDS, which was premixed with 1× protease inhibitor cocktail and 2 mM sodium vanadate. For tumor cell lysates preparation: after completion of *in vivo* experiment mice were sacrificed and small pieces of tumors were lysed in same buffer as described above. Respective cell lysates were run in different % of SDS-PAGE gradient gel according to antigen's molecular weight, and then the bands were transferred to Nitrocellulose membrane. BCIP/NBT was used for detection of protein bands by colorimetric method.

4.3. Statistical analysis

Data were expressed as the mean (SD) and statistically analyzed by the two-tailed, unpaired, Student's *t*-test using Microsoft Excel (Seattle, WA). For animal studies, scores were considered significant when $p < 0.05$. For in vitro studies, scores were considered significant when $p < 0.01$.

4.4. Software

Chemical structures were drawn with the help of ChemDraw software. For graph plotting Microsoft excel software was used. Images were prepared in Photoshop CS2.

Acknowledgment

SS acknowledges Council of Scientific & Industrial Research (CSIR), Govt. of India for his doctoral fellowship; RB acknowledges DST, Govt. of India [SR/S1/OC-64/2008] and CSIR Network Project 'ADD' [CSC 0302] for research support. Authors thankfully acknowledge Dr. Arabinda Chaudhuri, CSIR-IICT, India for his critical reading of the manuscript and providing valuable corrections and suggestions for the manuscript.

Abbreviations used

Dex	dexamethasone
TFA	trifluoroacetic acid
$NaIO_4$	sodium periodate
K_2CO_3	potassium carbonate
DCM	dichloromethane
GR	glucocorticoid receptor
GRE	glucocorticoid responsive element
Mdm2	mouse double minute 2
STAT3	signal transducer and activator of transcription 3
DMEM	DMEM Dulbecco's modified eagle medium
VEGFR2	vascular endothelial growth factor receptor 2
Bcl2	B-cell lymphoma 2
BAX	Bcl-2-associated X protein
XIAP	X-linked inhibitor of apoptosis protein
HOBT	1-hydroxybenzotriazole
DIPEA	diisopropylethyl amine
EDCI	1-Ethyl-3-(3-dimethylaminopropyl)carbodiimide.

Appendix A. Supplementary data

Supplementary data related to this article can be found at http://dx.doi.org/10.1016/j.ejmech.2014.06.051.

References

[1] J.D. Ashwell, F.W. Lu, M.S. Vacchio, Glucocorticoids in T cell development and function, Annu. Rev. Immunol. 18 (2000) 309–345.
[2] M. Reichardt, F. Tronche, S. Berger, C. Kellendonk, G. Schutz, New insights into glucocorticoid and mineralocorticoid signaling: lessons from gene targeting, Adv. Pharmacol. 47 (2000) 1–21.

[3] L. Frego, W. Davidson, Conformational changes of the glucocorticoid receptor ligand binding domain induced by ligand and cofactor binding, and the location of cofactor binding sites determined by hydrogen/deuterium exchange mass spectrometry, Protein Sci. 15 (2006) 722–730.
[4] A. McMaster, D.W. Ray, Drug insight: selective agonists and antagonists of the glucocorticoid receptor, Nat. Clin. Pract. Endocrinol. Metab. 4 (2008) 91–101.
[5] M. Beato, P. Herrlich, G. Schütz, Steroid hormone receptors: many actors in search of a plot, Cell 83 (1995) 851–857.
[6] S. Roux, B. Térouanne, P. Balaguer, N. Jausons-Loffreda, M. Pons, Chambon, H. Gronemeyer, J.C. Nicolas, Mutation of isoleucine 747 by a threonine alters the ligand responsiveness of the human glucocorticoid receptor, Mol. Endocrinol. 10 (1996) 1214–1226.
[7] R. Kofler, The molecular basis of glucocorticoid-induced apoptosis of lymphoblastic leukemia cells, Histochem. Cell Biol. 114 (2000) 1–7.
[8] S. Sharma, A. Lichtenstein, Dexamethasone-induced apoptotic mechanisms in myeloma cells investigated by analysis of mutant glucocorticoid receptors, Blood 112 (2008) 1338–1345.
[9] P.J. Hesketh, P.S. Altamira, Aprepitant, dexamethasone, and palonosetron in the prevention of doxorubicin/cyclophosphamide-induced nausea and vomiting, Support Care Cancer 20 (2012) 653–656.
[10] S.H. Shim, J.H. Hah, S.Y. Hwang, D.S. Heo, M.W. Sung, Dexamethasone treatment inhibits VEGF production via suppression of STAT3 in a head and neck cancer cell line, Oncol. Rep. 23 (2010) 1139–1143.
[11] H. Ge, S. Ni, X. Wang, N. Xu, Y. Liu, X. Wang, L. Wang, D. Song, Y. Song, C. Bai, Dexamethasone reduces sensitivity to cisplatin by blunting p53-dependent cellular senescence in non-small cell lung cancer, PLoS One 7 (2012) e51821.
[12] I. Herr, E. Ucur, K. Herzer, S. Okouoyo, R. Ridder, P.H. Krammer, M. von Knebel Doeberitz, K.M. Debatin, Glucocorticoid cotreatment induces apoptosis resistance toward cancer therapy in carcinomas, Cancer Res. 63 (2003) 3112–3120.
[13] A. Mukherjee, K.P. Narayan, K. Pal, J.M. Kumar, N. Rangaraj, S.V. Kalivendi, R. Banerjee, Selective cancer targeting via aberrant behavior of cancer cell-associated glucocorticoid receptor, Mol. Ther. 17 (2009) 623–631.
[14] K. Pal, S.K. Pore, S. Sinha, R. Janardhanan, D. Mukhopadhyay, R. Banerjee, Structure-activity study to develop cationic lipid-conjugated haloperidol derivatives as a new class of anticancer therapeutics, J. Med. Chem. 54 (2011) 2378–2390.
[15] S. Sinha, S. Roy, B.S. Reddy, K. Pal, G. Sudhakar, S. Iyer, S. Dutta, E. Wang, P.K. Vohra, K.R. Roy, P. Reddanna, D. Mukhopadhyay, R. Banerjee, A lipid-modified estrogen derivative that treats breast cancer independent of estrogen receptor expression through simultaneous induction of autophagy and apoptosis, Mol. Cancer Res. 9 (2011) 364–374.
[16] P.R. Muktapurama, R.K. Gara, K. Sharma, C. Rohit, K. Srinivas, D.P. Mishra, B.S. Reddy, Anticancer siRNA delivery by new anticancer molecule: a novel combination strategy for cancer cell killing, Eur. J. Med. Chem. 56 (2012) 400–408.
[17] H. Lin, W.M. Abida, R.T. Sauer, V.W. Cornish, Dexamethasone–methotrexate: an efficient chemical inducer of protein dimerization in vivo, J. Am. Chem. Soc. 122 (2000) 4247–4248.
[18] B. Giuseppe, A.T. Deborah, M.S. Jason, C. Louis, M. Lucas, D.J.P. Andrew, V.M. Tom, MDM2-p53 interaction in paediatric solid tumours: preclinical rationale, biomarkers and resistance, Curr. Drug Targets 15 (2014) 114–123.
[19] P. Pratheeshkumar, A. Budhraja, Y.O. Son, X. Wang, Z. Zhang, S. Ding, L. Wang, A. Hitron, J.C. Lee, M. Xu, G. Chen, J. Luo, X. Shi, Quercetin inhibits angiogenesis mediated human prostate tumor growth by targeting VEGFR-2 regulated AKT/mTOR/P70S6K signaling pathways, PLoS One 7 (2012) e47516.
[20] S. Saeed, B.D. Mohammad, M. Gholamreza, T. Mohammadreza, Role of Caspases, Bax and Bcl-2 in chrysin-induced apoptosis in the A549 human lung adenocarcinoma epithelial cells, Anti Cancer Agents Med. Chem. http://dx.doi.org/10.2174/1871520614666140209144042.
[21] E.H. Cheng, D.G. Kirsch, R.J. Clem, R. Ravi, M.B. Kastan, A. Bedi, K. Ueno, J.M. Hardwick, Conversion of Bcl-2 to a Bax-like death effector by caspases, Science 278 (1997) 1966–1968.
[22] Z. Gao, Y. Tian, J. Wang, Q. Yin, H. Wu, Y.M. Li, X. Jiang, Dimeric Smac/Diablo peptide directly relieves caspase-3 inhibition by XIAP dynamic and cooperative regulation of XIAP by Smac/Diablo, J. Biol. Chem. 282 (2007) 30718–30727.
[23] L. Ghibelli, M. Diederich, Multistep and multitask Bax activation, Mitochondrion 10 (2010) 604–613.
[24] E.S. Kandel, N. Hay, The regulation and activities of the multifunctional serine/threonine kinase Akt/PKB, Exp. Cell Res. 253 (1999) 210–229.
[25] J.R. Testa, A. Bellacosa, Akt plays a central role in tumorigenesis, Proc. Natl. Acad. Sci. U. S. A. 98 (2001) 10983–10985.
[26] S.R. Choudhari, M.A. Khan, G. Harris, D. Picker, G.S. Jacob, T. Block, K. Shailubhai, Deactivation of Akt and STAT3 signaling promotes apoptosis, inhibits proliferation, and enhances the sensitivity of hepatocellular carcinoma cells to an anticancer agent, Atiprimod, Mol. Cancer Ther. 6 (2007) 112–121.
[27] A.J. Levine, p53 the cellular gate keeper for growth and division, Cell 88 (1997) 323–331.
[28] A.J. Levine, J. Momand, C.A. Finlay, The p53 tumour suppressor gene, Nature 351 (1991) 453–456.
[29] R. Srinivas, A. Garu, G. Moku, S.B. Agawane, A. Chaudhuri, A long-lasting dendritic cell DNA vaccination system using lysinylated amphiphiles with mannose-mimicking head-groups, Biomaterials 33 (2012) 662–6229.
[30] S.K. Pore, A. Choudhary, B. Rathore, A. Ganguly, P. Sujitha, C.G. Kumar, S.B. Agawane, J.M. Kumar, V. Scaria, B. Pillai, R. Banerjee, Hsp90-targeted miRNA-liposomal formulation for systemic antitumor effect, Biomaterials 34 (2013) 6804–6817.